

# Understanding the joint impacts of soil architecture and microbial dynamics on soil functions: Insights derived from microscale models

Valérie Pot<sup>1\*</sup>, Xavier Portell<sup>2,3</sup>, Wilfred Otten<sup>2</sup>, Patricia Garnier<sup>1</sup>, Olivier Monga<sup>4</sup>, Philippe C. Baveye<sup>1</sup>

<sup>1</sup> Université Paris-Saclay, INRAE, AgroParisTech, UMR EcoSys, Thiverval-Grignon, France

<sup>2</sup> School of Water, Energy and Environment, Cranfield University, Cranfield, Bedfordshire, UK

<sup>3</sup> Departamento de Ciencias, IS-FOOD, Universidad Pública de Navarra, Pamplona, Spain

<sup>4</sup> IRD, UMI UMMISCO, Bondy, France

\* corresponding author: Valérie Pot – [valerie.pot@inrae.fr](mailto:valerie.pot@inrae.fr)

## Abstract

Over the last decades, a new generation of microscale models have been developed to simulate soil microbial activity. An earlier article (Pot et al., 2021) presented a detailed review of the description of soil architecture and microbial dynamics in these models. In the present article, we summarize the main results obtained by these models according to six model outputs: growth and spatial organization of microbial colonies, soil hydraulic conductivity, coexistence and trophic interactions of microorganisms, temporal dynamics of the amount of solid and dissolved organic matter in soil and, microbial production of CO<sub>2</sub>. For each of these outputs, we draw particular attention to the respective roles of soil architecture and microbial dynamics, and we report how microscale models allow for disentangling and quantifying them. We finally discuss limitations and future directions of microscale models in combination with the on-going development of high-performance imaging tools revealing the spatial heterogeneity of the actors of soil microbial activity.

## Highlights

- We review the insights on soil functions derived from microscale models of soil microbial processes
- Microscale models disentangle the complex interactions between soil architecture and microbial dynamics
- Spatial accessibility of resources to microbes, growth and ecological interactions are key factors in soil functions

31 • Translation of knowledge of interactions at the microscopic scale into larger scales is still in its  
32 infancy

33

34 **Keywords:** bacteria models, fungi models, spatial accessibility, ecological interactions, soil organic  
35 matter

36

## 37 **1. Introduction**

38 In the last two decades, a new generation of microscale models of soil microbial activity has been  
39 developed (e.g., Baveye et al., 2018 ; König et al., 2020 ; Pot et al., 2021). These models describe soil  
40 architecture at a small scale (from a few  $\mu\text{m}^3$  to a few  $\text{cm}^3$ ), as well as the heterogeneous distribution in  
41 it of trophic resources and microorganisms, and they account for soil-borne processes at the scale of  
42 soil microhabitats (Pot et al., 2021). In so doing, microscale models make it possible for users, through  
43 modelling scenarios, to explore the role of physico-chemical gradients and spatial accessibility of  
44 trophic resources to decomposers on soil microbial activity.

45 In Pot et al. (2021), we reviewed in detail how microbial dynamics and soil architecture are  
46 described in microscale models. Microscale models are defined by a computing grid of node size  
47 ranging between  $1 \mu\text{m}^3$  to  $1 \text{mm}^3$  where the physico-chemical environment, microorganisms, trophic  
48 resources and microbial products are spatialized. Box 1 visually depicts and explains how such models  
49 are used while Box 2 details an example of the use of the microscale model of Portell et al. (2018). In a  
50 nutshell, microscale models generally consider an explicit representation of microbial growth instead of  
51 a black-box approach that is widely adopted in the broader soil-related literature (e.g., Wieder et al.,  
52 2015). Measurable soil organic pools representing plant residues based on their degree of  
53 polymerization (non-labile polymers, labile monomers), biomass, and biomass by-products  
54 (metabolites, enzymes, glue agents, exo-polymeric substances) are described (e.g., Gras et al., 2011)  
55 rather than lumped organic matter (OM) pools based on their different degree of chemical recalcitrance  
56 to degradation. Most of the microscale models consider a depolymerization step before the dissolved  
57 OM can be taken up (e.g., Allison, 2005; Pagel et al., 2020; Zech et al., 2022), and this step can be  
58 controlled by the production of enzymes by microbes (e.g., Wang & Allison, 2019). Other models also  
59 include complex ecological interactions like commensalism, competition, mutualism (e.g., Folse &  
60 Allison, 2012; Wang & Or, 2014), fungal deadlock, intermingling, or replacement (e.g., Falconer et al.,  
61 2008), or bacterial dispersion through “fungal highway” (e.g., Banitz et al., 2011, 2016). Three-

62 dimensional images of soil architecture (mostly obtained from cutting-edge non-invasive imaging  
63 tools), informing on the geometry of the pore space and the spatial localisation of air-water interfaces,  
64 can be direct inputs for microscale models (e.g., Falconer et al., 2012). To decrease the amount of  
65 information needed in this detailed description of soil architecture, diverse strategies of simplification  
66 are used. Morphological models (e.g., Monga et al., 2014) and irregular pore-network models (e.g.,  
67 Perez-Reche et al., 2012) reconstruct simplified pore spaces by extracting the median axes of the  
68 imaged pores and filling the pores with well-defined geometrical forms (e.g., balls, cylinders, angular  
69 pores). Simpler (regular) pore-network models (e.g., Ebrahimi et al., 2014; Laudone et al., 2011, 2013)  
70 make use of statistical properties of pore connectivity and size defined according to values found in  
71 natural soil systems in order to reconstruct a simplified pore space. In these simplifications of the pore  
72 geometry, the exact spatial heterogeneity of the clustering of pores is lost. Finally, in contrast to these  
73 explicit approaches, another class of micromodels describes soil architecture in an implicit way by  
74 attributing lumped values of bulk porosity, water content and/or diffusion coefficient to the  
75 computational nodes of spatial grids (e.g., Folse & Allison, 2012). Whatever the level of detail of the  
76 soil architecture description contained in microscale models, different scenarios of spatial distribution  
77 of solid OM fragments, dissolved OM, physico-chemical gradients and microbes (bacteria and fungi,  
78 mostly) are proposed (e.g., Falconer et al., 2015; Ebrahimi & Or, 2015). Some of them are based on  
79 experimental data (e.g., Babey et al., 2017, Centler et al., 2011) whereas others use statistical models of  
80 the spatial distribution of bacteria (e.g. Pagel et al., 2020; Mbé et al., 2021).

81 Microscale models can thus lead to modelling scenarios where spatial interactions encompass  
82 optimal or low accessibility of OM to microbes, and thus can tackle how soil microbial activity is  
83 related to soil heterogeneity. However, these models face a number of limitations in describing the  
84 complexity of soil architecture and microbial life. Most of them describe a static soil architecture  
85 although innovative studies have attempted to investigate the feedback loops between architecture and  
86 microbes (Crawford et al., 2012 ; Ray et al., 2017) or roots (Aravena et al., 2014 ; Kolb et al., 2017)  
87 and physico-chemical processes (Rupp et al., 2019). Regarding ecological interactions, a number of  
88 simplifications have been undertaken, such as, among others, a simplification of soil biodiversity and  
89 an omission of the role of living roots (Pot et al., 2021). Although the research on the role of trophic  
90 regulation in soils has made important progress (Erktan et al., 2020), predation has not been explicitly  
91 included in microscale models, except for the model of Pagel et al. (2020).

93 **Box 1:** Space is at the heart of microscale models of soil functions. Soil architecture is accounted for mainly  
94 following two types of spatial description: explicit and implicit (Figure 1). The explicit description relies on a  
95 representative image of soil architecture (for example a CT image) from which the solid phase and the pore  
96 space is extracted. Other phases such as water and organic matter can also be imaged to some extent. Pore space  
97 is either directly implemented at the nodes of the model grid – using a regular mesh or finite element (FE) or  
98 finite volume (FV) meshing – or simplified by using geometrical approaches (for example Maximal Inscribed  
99 Balls) or pore network models (PNM). The spatial distribution of air/water interfaces, microorganisms, and OM  
100 (solid or dissolved) are added to the explicit description of the pore space. In some circumstances, these  
101 distributions can be measured using imaging tools ( $\mu$ CT, neutron CT, synchrotron  $\mu$ CT, 2D microscopy, ...) but,  
102 more often, they are computed. For example, the Young-Laplace law can be used to water fill or empty pores  
103 and statistical models can be used to distribute microorganisms in the pore space, or meaningful scenarios can  
104 be used. Alternatively to the explicit approach, an implicit description of soil architecture can also be adopted. In  
105 this implicit approach, the bulk values of porosity, water content and effective molecular diffusion coefficient –  
106 measured on the considered soil samples or calculated from semi-empirical laws – are distributed at the grid  
nodes made of a regular mesh. Spatial heterogeneity of these variables can be generated by statistical models or  
scenarios.

107 In microscale models, microbial activity is accounted for explicitly (Figure 1). Solid OM pools are  
108 depolymerized in labile components (DOC) to be taken up by microorganisms. Ecological interactions,  
109 including competition for resources, mutualism or commensalism can be this way easily implemented by  
establishing relationships between different OM pools.

110 Coupling between the soil architecture and microbial dynamics (purple arrows in Figure 1) is achieved through  
111 the transport of the soluble and gaseous components (DOC, enzymes, emitted gases) and the microorganisms in  
112 pore space (via processes of diffusion, advection, colonization of fungal hyphae and bacterial chemotaxis or  
random movement).

113 Finally, the outputs of microscopic models can generally be divided at two levels (Figure 1): (i) spatialized  
114 output variables at different output times of the models, and (ii) temporal evolutions of these output variables  
115 averaged over the entire simulated domain.

116

117

118

119

120

121

122

123

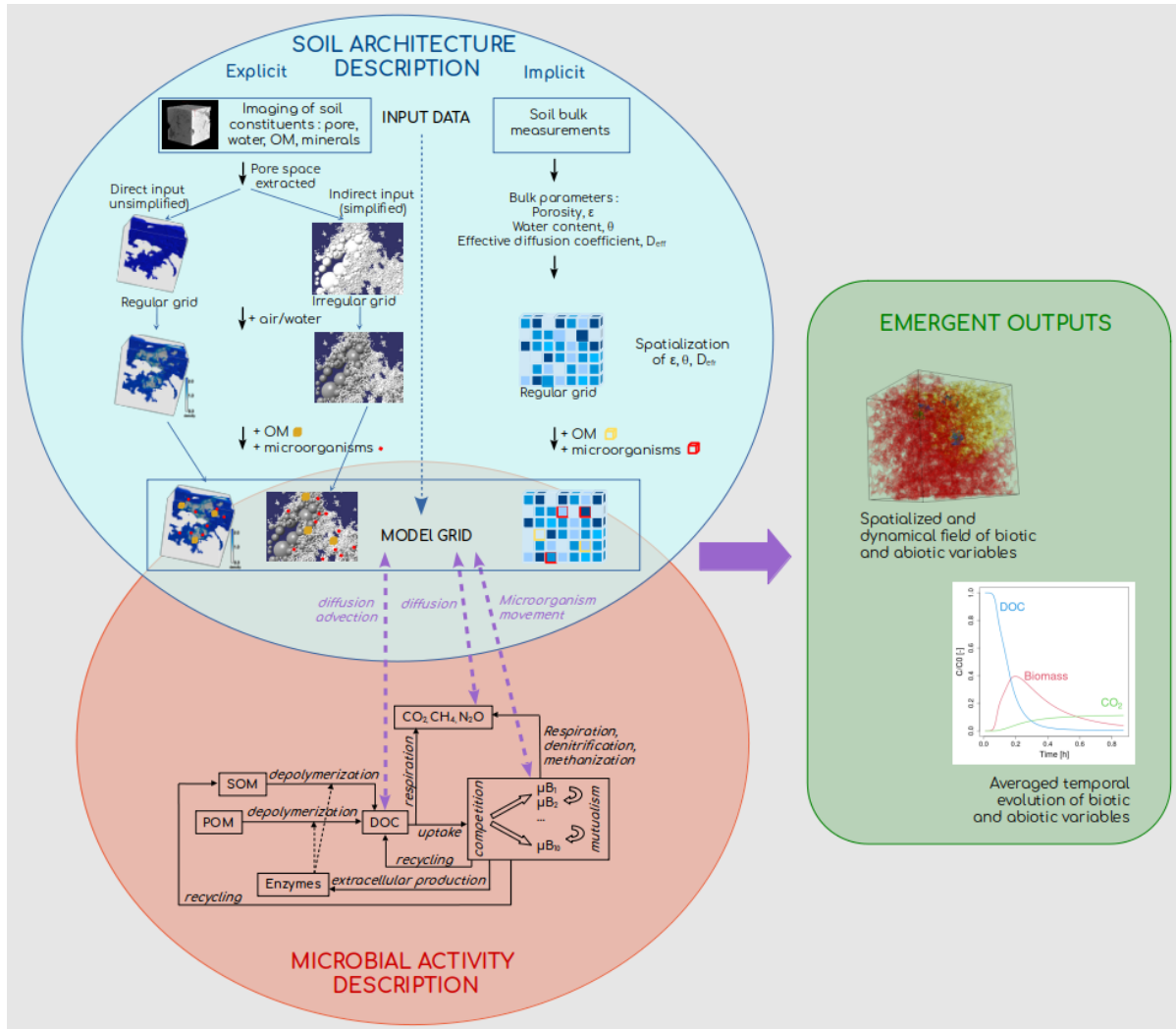


**Figure1:** Main set-up characteristics of microscale models of soil functions.

124  
125  
126

127 In that general context and to complement the review of Pot et al. (2021), we summarize in the  
128 present review the main insights gained by this new generation of microscale models on the  
129 understanding of soil functions. These new insights relate to the emergence of a spatial organization of  
130 microbial (bacteria and fungi) colonies (Section 2.1), its consequence on the hydraulic conductivity in  
131 idealized porous media (Section 2.2), coexistence and trophic interactions (Section 2.3), and finally, the  
132 decomposition of solid and dissolved OM and the emission of CO<sub>2</sub> (Section 2.4). We then describe how  
133 microscale models can disentangle the role of soil architecture and microbial dynamics (Section 3) and  
134 we finally discuss issues related to the assessment of these models and upscaling and advocate for  
135 future directions (Section 4).

**Box 2:** Example of microscale modelling study tackling bacterial diversity. The IbLBioS microscale model of Portell et al. (2018) couples a lattice-Boltzmann approach – to describe the diffusion of dissolved organic carbon hydrolyzing from particulate organic matter (POM) – with an individual-based model – to describe bacterial dynamics (Figure 2A). It assumes an explicit description of soil architecture using X-ray  $\mu$ CT images describing the solid phase and pore space. The water distribution is computed using a two-phase lattice-Boltzmann model for three levels of water saturation ( $S_w=100\%$ ,  $50\%$  and  $25\%$ ). 690 initial bacteria having parameter combinations representative of competitive, poorly competitive and versatile *Arthrobacter* Sp. Strains are randomly distributed in the water phase (Figure 2B). The role of spatial accessibility of OM to bacteria is accounted for with three scenarios initializing a fixed amount of carbon distributed in one chunk of POM, four chunks of POM and already available as DOC (Figure 2C). The main outputs studied by the authors were the time evolutions of the averaged POM and DOC amount,  $CO_2$  production, biomass of the bacterial strains and the growth observed in the bacterial microcolonies (Figure 2D). In addition, they computed the geodesic distance between these microcolonies and the POM chunks.

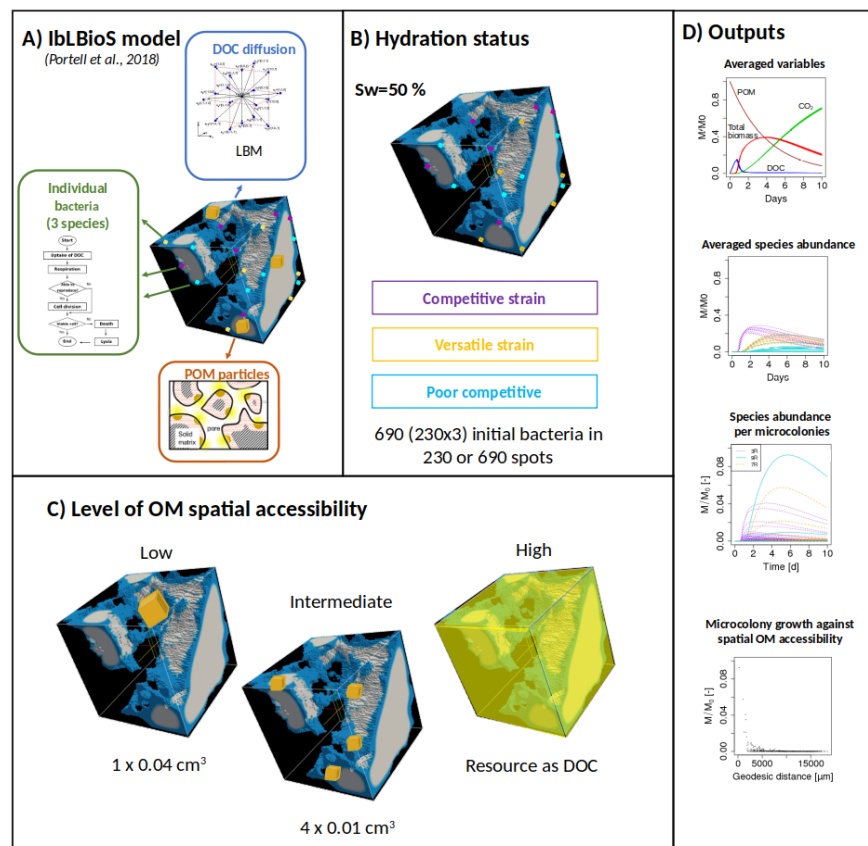


**Figure 2:** Overview of the main steps of modelling scenarios with a microscale model.

## 2. Main insights derived from microscale models

### 2.1 Spatial organization of soil microbial colonies

#### 2.1.1 Case of bacteria

In modelling scenarios based on an implicit approach to describe soil architecture, Folse & Allison, (2012) developed an individual-based model that considers competition, coalition, and cooperation between different genotypes of a bacterial species. The microbes feed on carbon-, nitrogen- and phosphorous-containing substrates that are distributed on a 2D grid. These substrates need to be hydrolyzed by substrate-specific enzymes in order to be available. Bacteria that produce extracellular enzymes and opportunists or cheaters that do not produce such enzymes are initially randomly distributed on the 2D grid. Unlike the enzymes and the bacteria, the C, N, and P substrates do not diffuse on the grid. The heterogeneity of soil architecture is not investigated and an effective diffusion coefficient is assigned to the enzymes. Given these assumptions, Folse and Allison, (2012) found that the spatial organization of bacteria varies with enzyme diffusion and production rates. Following the same approach, König et al. (2017, 2018, 2019) located disturbance events at random microsites on the computational grid. These events, consisting of a decrease in biomass, modify the spatial structure of the bacterial communities and lead to habitat fragmentation. The spatial characteristics of the disturbances (size and degree of fragmentation) influence the resilience of the system by affecting the ability of bacteria located in undisturbed areas to recolonize disturbed areas. In these modeling scenarios, an effective diffusion coefficient is attributed to bacteria. The dynamic of the spatial structure of bacterial colonies is controlled by threshold effects and high growth rate is identified as an asset for recovery in the case of medium intensity disturbances

Using an explicit but simplified 3D description of soil architecture, Resat et al. (2012) involved enzyme producers and cheaters that feed on two cellulose patches placed in distinct zones of the computational grid. They came to the same overall conclusions as Folse and Allison (2012). The bacterial growth dynamics relies on a balance between the degradation kinetics of the substrate (in this case cellulose), the dynamics of enzyme production, and the mixing in pores by diffusion. The model predicts that bacteria preferentially grow near cellulose spots. Surprisingly, Resat et al. (2012) found similar growth dynamics, except for a shift in time, from those obtained in single cylindrical micropores. Growth remains also insensitive to modification of the porosity of the porous medium, although it is varied over a significant range (20% to 50%). One explanation is that the artificial and

197 highly connected pore network of the simulated domains may have prevented critical cases of diffusion  
198 limitation.

199 The role of chemotaxis on the emergence of different spatial patterns is explored by Gharasoo et al.  
200 (2014) who compared 2D simplified soil architectures considering pore networks made of cylindrical  
201 bonds of either constant radius or variable radius. When the supply of substrate is constant and  
202 homogeneous, bacterial distribution remains uniform in the presence of chemotaxis toward the  
203 substrate (Gharasoo et al., 2014). When bacteria are further attracted by the presence of fellow bacteria,  
204 spatial organization emerges. Increasing the strength of chemotaxis towards bacteria triggers non-trivial  
205 populations in a homogeneous porous medium. In the heterogeneous porous media, a distribution of  
206 pluri-millimeter size patches emerges when attraction to nutrient is low and bacteria tend to migrate  
207 from larger pores toward smaller pores. The authors conclude that the distribution of bacteria in soil is  
208 strongly related to the chemotactic behavior of the bacteria.

209 The additional role of water hydration status of pores in the emergence of distinct spatial  
210 organizations of bacteria is evidenced in different levels of description of soil architecture. Using pore  
211 networks made of angular bonds to describe 2D and 3D analogs of soil aggregates, Ebrahimi and Or  
212 (2014) showed that when the water content is high enough to ensure a high connectivity, chemotaxis  
213 toward substrate makes it possible to favor the shortest paths to the source of nutrients, and avoid  
214 tortuous paths associated with random displacements. In the case of many isolated clusters, chemotaxis  
215 has the opposite effect, as it can guide bacteria to dead-end pores, and travel times can become longer  
216 than required for random movements (Ebrahimi & Or, 2014). In the case of an explicit description of  
217 an idealized 2D soil architecture representing porous rough surfaces (Long & Or, 2007), microscale  
218 models predict a larger annular expansion of a bacterial colony under wet conditions (matric potential  
219 of -0.01 kPa) compared to drier conditions (matric potential of -1 to -2 kPa). These spatial patterns are  
220 the result of an interplay between nutrient diffusion limitation and motility of the bacteria. The inner  
221 center becomes rapidly depleted in nutrients because of the local consumption by bacteria therein but  
222 also because of the interception of the nutrients by bacteria located at the periphery of the colony. The  
223 different patterns observed between the saturation conditions are accounted for by a decrease of the  
224 connectivity of the water phase due to the fragmentation of the liquid phase and to the slowing down of  
225 the diffusion of nutrients (Wang & Or, 2010). Using a 2D implicit description of the porous rough  
226 surfaces, Kim and Or (2016) found that the spatial structure of two bacterial colonies is modified by the  
227 water hydration status and ecological interactions. In the case of competitive trophic interactions, the



228 two species segregate along circular “travelling bands”. Species 1 follows species 2 and consumes the  
229 nutrients left by species 2. Under dry conditions, the double bands disappear and form a unique band  
230 made of several small sectors of the same species. In this case, diffusion of the nutrients is reduced and  
231 the species need to compete to remain at the front line. In the case of mutualistic interactions, under wet  
232 conditions, species 1 grows better than species 2, which consumes the by-product of species 1, whereas  
233 the reverse is observed for dry conditions.

234 The role of the spatial distribution of carbon substrate also appears to be key to account for the  
235 spatial organization of aerobic and anaerobic species in 3D analogs of soil aggregates. In modelling  
236 scenarios carried out by Ebrahimi and Or (2015), the same number of aerobic and anaerobic bacterial  
237 cells are inoculated in the center of the aggregate. A constant O<sub>2</sub> concentration is supplied at the  
238 periphery of the aggregate, while the carbon source is located either at the center of the aggregate or at  
239 the periphery. A spatial organization with physical separation of the two species occurs between the  
240 anoxic center of the aggregate and the oxygenated periphery (Ebrahimi & Or, 2015). Borer and Or  
241 (2018) further confirmed, in simulated domains mimicking experimental micrometric pore networks  
242 etched in glass, that the absence of counter-gradients of oxygen and carbon resulted in a uniform  
243 distribution of aerobes and anaerobes. However, the distribution is conditioned by the presence of a  
244 carbon source internal to the aggregate. In the absence of this source, the anaerobic species does not  
245 survive (Ebrahimi & Or, 2015). The size of the aggregate is also a key factor in the distribution and  
246 maintenance of the two species (Ebrahimi & Or, 2016). Using a simplified 2D description of soil  
247 analogs, Borer et al. (2019) introduced a metabolic flexibility where the anaerobes can grow in both  
248 aerobic and anaerobic environments by adapting their metabolism. This adaptation permits the spatial  
249 segregation of the facultative anaerobes into an aerobic population growing close to the oxygen  
250 peripheral source and an anaerobic population close to the internal carbon source.

251 In conclusion, the reported modelling studies show that the spatial distribution of bacterial colonies  
252 can differ strongly, depending on the interplay between factors related to spatial accessibility of OM  
253 and O<sub>2</sub> to bacteria, and factors related to microbial dynamics. The former factors are the heterogeneity  
254 of soil architecture, water content, substrate spatial distribution and chemotactic behavior of bacteria.  
255 The latter factors are the growth rate of bacteria, their enzyme production rate, and ecological  
256 interactions which are directly related to the efficiency of bacteria to consume OM.

257

258

### 2.2.2 Case of fungi

259

260 The role of soil architecture in the invasion of fungi-like microbes is highlighted by a series of  
261 modelling scenarios (Perez-Reche et al., 2012) where the pore space is described using an irregular  
262 pore-network model made of nodes and links (pores) distributed in a way that preserves the spatial  
263 distribution and width of the pore arrangement. Invasion of microbe analogs is carried out through a  
264 generic probabilistic model that could resemble fungal invasion (Bailey et al., 2000) and growth is not  
265 considered. The probability for a microbe to invade a new pore is constrained by the length but also by  
266 the width of the links. Perez-Reche et al. (2012) demonstrated that the inclusion, in their pore-network  
267 model, of the extra complexity of the width of the links has a significant impact on the ability of  
268 microbe to invade the soil sample. The invasion distance is underestimated when the lengths and width  
269 of the links but also the number of nodes are not sufficiently considered in the invasion probability.  
270 Bailey et al. (2000) and Otten et al. (2001) showed how fungal colony morphology can be linked to  
271 such probabilities and tested the approach in experimental 2D systems with localized C sources (Otten  
272 et al., 2004a) on a lattice as well as for spread of a pathogen through a population of plants (Cook et al.,  
273 2007).

274 Assuming an idealized soil architecture made of different proportions of solid and porous nodes and  
275 addressing the complexity of fungal processes, i.e., by including substrate uptake, hyphal tip growth,  
276 branching, Boswell (2008) showed that the simulated biomass length and the total number of hyphal  
277 tips decrease as the density of soil increases. The hyphal growth unit, which is the total mycelial length  
278 divided by the number of branches in the mycelium, is the greatest in dense soils. These results agree  
279 with the visual observations made by Harris et al. (2003) in soil thin sections (Otten et al., 2006). One  
280 explanation would be that the fungus has less opportunity to branch when the pore space is reduced as  
281 observed by Otten et al. (1999) and Soufan et al. (2018). In another set of modelling scenarios where  
282 detailed soil architecture is considered through the use of CT images of sandy soil samples repacked at  
283 different densities, Pajor et al. (2010) also found that the colonization rate of the fungus is highest for  
284 the repacked sandy soils with the lowest density. Indeed, fungal biomass spreads faster and further in  
285 better-connected soil (Otten et al., 2006). The model of Pajor et al. (2010), which is derived from that  
286 of Falconer et al. (2007), describes the invasion of fungal hyphae according to a diffusion process and  
287 this explains the fact that a well-connected pore space is ultimately colonized. The total porosity of the  
288 domain is then the key factor explaining the spatial expansion of the fungus. However, if the pore  
289 connectivity decreases, the fraction of pores colonized with distance declines more rapidly than in a

290 well-connected pore space. In this case, it is the connectivity of the pore space that becomes the key  
291 factor explaining the spatial expansion of the fungus. The results of Pajor et al. (2010) agree with the  
292 experimental results of Harris et al. (2003) who showed that the hyphae initially colonize the largest-  
293 sized pores, followed by colonization of smaller pores. Nevertheless, the model overestimates the  
294 spread of hyphae in the small pores compared to the experimental results of Otten et al. (2004b). A  
295 more heterogeneous distribution of carbon or the result of blockage of small pores by the presence of  
296 water in the experiments may explain these differences. Indeed, in the scenarios of Pajor et al. (2010),  
297 all pores are assumed to be filled with air. Kravchenko et al. (2011) modelled fungal colonization in  
298 detailed soil architecture obtained from CT images of undisturbed soil samples. They also showed that  
299 the fragmented pore space disadvantages fungal invasion whereas large connected pores promote  
300 invasion.

301 The spread of fungal hyphae is also directly dependent on the initial distribution of the substrate  
302 since the complex arrangement of pores imposes constraints on the accessibility of resources to the  
303 fungus. This relationship is further influenced by the complexity of fungal processes, as demonstrated  
304 in modelling scenarios describing either idealized (Boswell et al., 2007) or detailed soil architecture  
305 obtained by CT images of soil samples (Cazelles et al., 2013). When carbon is co-located with the  
306 inoculum, the fungus consumes the local resource resulting in an increase in its biomass there and a  
307 smaller spatial expansion in the soil than for a homogeneous distribution of the resource (Cazelles et  
308 al., 2013). Biomass recycling, which reallocates biomass through the mycelium and favors faster  
309 growth and an exploratory behavior of the fungus, is an effective strategy to compensate for  
310 heterogeneous distributions of the substrate in a complex porous medium (Boswell et al., 2003;  
311 Boswell et al., 2007; Cazelles et al., 2013; Falconer et al., 2007).

312 A significant decrease in the growth of the fungus is observed in relation to water unsaturated  
313 conditions (Falconer et al., 2012). The spatial expansion is prevented by the presence of pores filled  
314 with water, which strongly alters the connectivity of the air phase. Simulations of fungal growth in two  
315 soil samples of contrasted pore space geometry interestingly shows that it is not the sample with the  
316 largest water content that inhibits the most the fungal colonization. More important than the water  
317 content is the location of the water filled pores that disconnect the gas phase. Water films that contain  
318 nutrients can also guide fungi to colonize pore space and find new resources (Boswell et al., 2007). The  
319 macroscopic water content of soil samples is therefore not a sufficient measure to predict the growth  
320 and spatial expansion of the fungus. Knowledge of the heterogeneity of the soil microhabitats and in

321 this case of the distribution of water and air in the pores and the connectivity of the air phase, is  
322 therefore essential (Falconer et al., 2012). This role of unsaturated pores has been observed in  
323 microfluidic devices by Soufan et al. (2018).

324 The role of soil architecture combined with ecological interactions is evinced in the spatial  
325 distribution of two fungal colonies (Falconer et al., 2008). The model simulates complex fungal  
326 deadlock (inhibited invasion of one species into the territory of the other species), intermingling (fusion  
327 of fungal colonies) and replacement (autophagy) processes. In agreement with the experimental results  
328 of Stahl and Christensen (1992), the deadlock and intermingling processes occur for environments with  
329 high and low trophic resources respectively in absence of soil architecture. When simplified soil  
330 architecture is described, the two colonies inoculated at the opposite edges of the simulated domain  
331 only manage to cross the domain for a defined porosity interval (0.31-0.55) because connected paths  
332 between opposite edges are numerous enough for individuals to cross while avoiding each other. It is  
333 important to notice that these simulations were in a 2D space where fungal colonies spreading from  
334 opposite directions are always going to meet. This in contrast for soil where, for soils with low pore  
335 connectivity, colonies can grow past each other in different sections of the 3D pore volume.

336 Like for bacteria, spatial colonization by fungi is explained by a balance between the accessibility of  
337 trophic resources (which depends on the connectivity, size and water saturation of pores), and the  
338 physiological characteristics of fungi, such as their biomass recycling and ecological interactions .

339

## 340 **2.2. Modification of hydraulic conductivity in idealized porous media**

341 Biofilms, i.e., a continuous layer of accumulated biomass and its metabolic by-products along the  
342 pore-solid interfaces, can be found in artificial porous media during industrial processes of filtration.  
343 Most of the reported modelling studies simulating this process carry out scenarios in idealized porous  
344 media usually consisting of packings of cylinders or glass beads. A reduction of global permeability of  
345 these idealized porous media is observed during growth of these biofilms together with the creation of  
346 preferential water flow paths (e.g., Graf von der Schulenburg et al., 2009 ; Kapellos et al., 2007 ;  
347 Tartakovsky et al., 2009). The shear forces prevent the development of biomass in the pores oriented in  
348 the transverse flow direction even if the local concentrations of the trophic resources in these pores  
349 would allow bacterial development (Knutson et al., 2005). Feedback loops emphasize this pattern since  
350 bacteria that are more concentrated close to preferential flow paths consume more food than in the case  
351 of more homogeneous flow fields and thus leave less food for the bacteria cells located farther,

352 reducing transverse expansion (Tang et al., 2013). Bioclogging of pores differently affects water flow  
353 reduction and is controlled by the water saturation of pores (Rosenzweig et al., 2013).

354 Inclusion of more complex processes in microscale models changes the picture one gets of the  
355 spatial proliferation of bacteria. When detachment processes of bacterial cells from biofilms are  
356 considered in microscale models, the spatial expansion of bacteria downstream of the water flow  
357 increases (Kapellos et al., 2007). In this case, detached cells are transported by advection and are  
358 redeposited farther downstream, forming new colonies. When motility of bacteria occurs via diffusion  
359 against local solute concentration gradients, localized accumulations of bacterial cells are reported in  
360 regions of more stagnant flow (Peszynska et al., 2016). When permeability in biofilms is introduced,  
361 the shear forces at the biofilm-water interface are reduced and cell re-attachment to the biofilm surface  
362 is enhanced (Kapellos et al., 2007).

363 Whereas the above examples are all dealing with artificial porous media and have applications that  
364 do not directly involve soils (for more details, see the recent review by Sadeghnejad et al. (2021)), they  
365 address important interactions that occur as well within soil environments but have yet to be captured  
366 by microscale models designed to describe and predict soil functions. Local accumulation of biomass  
367 and its metabolic by-products in soils, although not in the form of continuous biofilms (Baveye, 2020;  
368 Flemming et al., 2021), can contribute to preferential flow paths. Feedback loops emerge that alter pore  
369 geometry, which in-turn alters physical processes that impact biomass growth. The extent to which this  
370 phenomenon, referred to by Crawford et al. (2012) as self-organization of soil systems, is implemented  
371 in soil microscale models remains limited at this stage (Crawford et al., 2012; Ray et al., 2017), but it  
372 seems fair to consider that much can be learned from the studies referred to above.

373

### 374 **2.3. Coexistence and trophic interactions of microorganisms**

375 Soils are known to be characterized by an enormous biodiversity (e.g., Baveye et al., 2016). Because  
376 of computational limitations and especially of a fundamental lack of relevant input data, microscale  
377 models cannot reflect that biodiversity. However, they are able to capture key factors controlling the  
378 survival and/or coexistence of a limited number of meaningful functional groups of microbial species.  
379 When soil architecture is not explicitly described and a single value of effective diffusion coefficient is  
380 used throughout the simulated domain, survival and coexistence of simulated species is mainly  
381 attributed to a balance between the rates of production of enzymes by communities experiencing  
382 different ecological interactions (competition, coalition, and cooperation) and the rates of enzyme

383 diffusion (Folse & Allison, 2012). When considering local spatial heterogeneity in porosity and water  
384 content in their simulated domain, Long and Or (2005) identified the key role of local  
385 microenvironments conditions on survival and coexistence of two bacterial species (one more  
386 competitive than the other) for the same trophic resource. The coexistence of the species is made  
387 possible for low water contents, whereas the less competitive species becomes extinct under conditions  
388 when diffusion is not limiting. The fragmentation of aquatic habitats shelters less competitive species  
389 and sustains nutrient gradients. When the least competitive bacterial colonies are located near active  
390 diffusion paths, they can survive and thus compensate for their disadvantage in terms of competition  
391 with respect to the most competitive species (Long & Or, 2005). Under wet conditions, the motility of  
392 bacteria accelerates extinction due to a higher local expansion of the most competitive species that  
393 intercepts the available nutrients (Wang & Or, 2013). However, drier conditions reduce the role of  
394 motility, which decreases sharply even for the most competitive species (Long & Or, 2009). Variably  
395 water-saturated conditions can counterbalance negative effects on the survival of the least competitive  
396 species and thus promote biodiversity (Wang & Or, 2013). In modelling scenarios of wetting and  
397 drying cycles, Wang and Or (2013) found similar growth dynamics for both species. These results are  
398 consistent with experimental results on bacterial diversity that is not affected by wetting and drying  
399 cycles in soils regularly subjected to these cycles (Fierer et al., 2003).

400 Using a detailed description of soil architecture obtained from CT images of undisturbed soil, Portell  
401 et al. (2018) found that the spatial distribution of OM residues has an important role in shaping  
402 bacterial diversity in the case of three bacterial strains, a competitive, a generalist, and a poorly  
403 competitive one, for the same trophic resource. Whereas at the scale of the whole simulated domain,  
404 the evolution of the total biomass is not affected by the location of OM, the evolution of the biomass of  
405 each strain is strongly modified. When the residues are gathered in a unique location, the less  
406 competitive strain can grow as much as the generalist strain. In these rare cases, the probability of  
407 being near the unique carbon source is lower but, when this happens, the large amount of dissolved  
408 organic carbon produced by the aggregated residues can provide an advantage and promotes the growth  
409 of the less competitive strain. These results confirm those of Long and Or (2005) on the critical role of  
410 spatial location of colonies near active diffusion pathways. In addition, Portell et al. (2018) also found  
411 that the least competitive strain cannot grow if it is co-located with a competitive strain even when they  
412 are located near the resource. The proximity of bacteria to residues is thus not sufficient to maintain  
413 biodiversity, the less competitive strain must also not be co-located with a competitive strain.

414 Microscale models, in exploring the labyrinth of pores, have provided valuable insight into key  
415 factors maintaining soil bacterial biodiversity. While ecological interactions are crucial, the occurrence  
416 of transient water saturated conditions in soils, by fragmenting the complex aquatic habitats of bacteria,  
417 and the heterogeneous spatial distribution of trophic resources, offer sufficiently diverse ecological  
418 niches where less competitive species can survive.

419

## 420 **2.4. SOM decomposition and CO<sub>2</sub> emission**

### 421 **2.4.1 Role of soil architecture, spatial distribution of OM and microbes**

422 Respiration rates are highly influenced by the connectivity of pores. Using a detailed description of  
423 soil architecture obtained from CT images of soil columns, Yan et al. (2016) simulated lower  
424 respiration rates in denser soils. In their microscale model, the role of oxygen is considered in bacterial  
425 growth together with diffusion of O<sub>2</sub> in liquid and gaseous phases. In denser soil with poorer  
426 connectivity, OM is less accessible to bacteria, O<sub>2</sub> is limited by gaseous diffusion and this explains the  
427 lower respiration rates (Yan et al., 2016). This is in agreement with the experimental results of  
428 Franzluebbers (1999) who showed that carbon and nitrogen mineralization is generally lower in  
429 compressed soils compared to natural soils. However, pore connectivity does not alone explain the  
430 SOM decomposition and respiration rates that were found. There are complex relationships depending  
431 on the spatial distribution of OM and bacteria within soil architecture. For example, in the case of the  
432 modelling scenarios of Mbé et al. (2021), mineralization of OM decreases when soil bulk density  
433 increases in the case of aggregated bacteria distribution whereas it is similar when bacteria are  
434 homogeneously distributed.

435 A convenient feature of microscale models is their ability to control the distribution of OM and  
436 microbes in the simulated soil architecture. Different modelling scenarios have been proposed to test  
437 how spatial accessibility of OM to bacteria influence SOM decomposition and CO<sub>2</sub> production at the  
438 scale of the entire simulated domain. Modelling scenarios can be established based on experimental  
439 results relating the distribution of OM and bacteria to the size of pores. For example, Strong et al.  
440 (2004) found that the most active and largest bacterial population is found in the pores of class 15-60  
441 µm and Lugato et al. (2009) found that the organic carbon of the soil is positively correlated with pores  
442 of size 0.1-5 µm and negatively correlated with pores of size 30-75 µm. Following these experimental  
443 findings, Ngom et al. (2011) carried out modelling scenarios where OM is placed in pores smaller than  
444 20 µm and bacteria are distributed in larger pores because they are the most aerated. Up to a two-fold

445 amount of OM is mineralized in grass land soil aggregates that exhibit much less small, isolated pores  
446 than in cultivated plowed soil aggregates, because OM is then more accessible to bacteria.

447 Other scenarios do not relate the spatial distribution of OM and bacteria to the size of pores but  
448 compare dispersed (random) versus aggregated spatial distributions of OM residues and/or bacterial  
449 cells. A reduction in CO<sub>2</sub> production in the long term is observed in the case of an increase in the  
450 aggregation of bacterial spots (Masse et al. 2007). In these scenarios, decomposition takes place only  
451 when there is a physical contact between the bacterial spots and the OM patches that are placed in a  
452 minimalist 3D space where pore geometry and diffusion processes are ignored. The number of bacterial  
453 spots no longer having access to OM increases sharply and this is enough to reduce the overall carbon  
454 mineralization. Similar results are obtained with a more accurate description of soil architecture. Mbé  
455 et al. (2021) used a morphological approach to describe the pore space of repacked sandy loam soil  
456 samples obtained from CT images. Their microscale model considers diffusion of dissolved carbon in  
457 the liquid phase. For a homogeneous distribution of dissolved OM, Mbé et al. (2021) found lower  
458 mineralization when bacteria are aggregated compared to scenarios where bacteria are homogeneously  
459 distributed. In the latter case, there is a greater accessibility of bacteria to the trophic resource. In a  
460 simplified 1D geometry representing an experimental micromodel, Centler et al., (2011) also found that  
461 degradation efficiency is the highest for homogeneous bacteria distribution and decreases as pattern  
462 formation of bacteria sets up. Aggregation of bacteria stems from the introduction of flagellated  
463 movement and chemotaxis toward nutrient and toward chemo-attractant produced by the bacteria.  
464 Increasing the chemotaxis strength toward substrate or fellow bacteria reduces further the total biomass  
465 and degradation activity in the case of aggregated distributions of bacteria (Gharasoo et al., 2014). All  
466 these modelling results agree with the experimental data of Dechesne et al. (2010) who showed lower  
467 substrate mineralization rates for aggregated bacterial distributions.

468 For random distributions of bacterial spots, an increase in the aggregation of OM patches increases  
469 mineralization (Mbé et al., 2021) but also the variability among repetitions (Masse et al., 2007; Nunan  
470 et al., 2020). Although access to the trophic resource becomes increasingly limited, the amount of OM  
471 to which some bacteria have access remains sufficient to produce greater mineralization in the long  
472 term. When both spatial distribution of bacteria and OM are aggregated, mineralization is not ranked  
473 against the degree of clustering of OM or bacteria (Mbé et al., 2021). Results are highly influenced by  
474 the occurrence of co-localization of bacterial hot-spot with large plant residues containing a high  
475 amount of OM which can even surpass mineralization of a random distribution of OM (Mbé et al.,



476 2021). All these modelling results agree with the experimental measurements of Bending and Turner  
477 (1999) who showed a greater emission of CO<sub>2</sub> in the presence of large chunks of plant residues.  
478 However, they are in apparent contradiction with experimental results that have shown that large plant  
479 residues, having a high C/N ratio, cause less mineralization than smaller residues. In these experiments,  
480 the soil N bioavailability is probably increased by a more even distribution of residues in the soil and a  
481 higher contact surface for smaller residues (e.g., Angers & Recous, 1997; Tarafdar et al., 2001). In the  
482 scenarios of Portell et al. (2018), where N is unlimited, the OM residues are positioned in such a way  
483 that the contact surface is always identical whatever their aggregation. The production of dissolved  
484 organic carbon (DOC) by hydrolysis of these residues is a constant rate per unit surface that leads to  
485 similar global CO<sub>2</sub> emissions and DOC consumption. In the scenarios of Masse et al. (2007) the contact  
486 surface decreases when the degree of aggregation increases. However, aggregation also causes an  
487 increase in the amount of carbon available for bacterial spots and results in a higher available amount  
488 of OM explaining the highest CO<sub>2</sub> emissions. However, using the same model of Masse et al. (2007),  
489 mineralization decreases when the size of the plant residue increases in the case of N limitation  
490 (Garnier et al., 2008).

491 The emission of CO<sub>2</sub> through fungal activity is also directly related to nutrient access, itself  
492 controlled by pore connectivity. Higher CO<sub>2</sub> emissions are simulated for scenarios where carbon is co-  
493 located with the inoculum (Cazelles et al., 2013). On the contrary, in the homogeneous distribution of  
494 carbon throughout the pore space, the fungus must expand to have total access. This results in a lower  
495 assimilation of biomass and a lower respiration. A non-linear relationship between respiration of fungi  
496 and amount of solid OM residues has been found (Falconer et al., 2015). In these scenarios, the impact  
497 of the distribution of OM but also their size and amount of carbon is considered. For small amounts of  
498 carbon in the OM residues, the fungus biomass decreases and the amount of accumulated CO<sub>2</sub>  
499 stabilizes. Above critical thresholds of the amount and size of OM residues (3% of carbon and 60%  
500 coverage of the solid-pore interface by OM, respectively), the cumulative CO<sub>2</sub> follows an exponential  
501 growth over time. In addition, Falconer et al. (2015) observed a difference between replicated samples  
502 up to a factor of 100 between the amounts of cumulative CO<sub>2</sub> for different sizes of OM. Respiration is  
503 the largest but also the most variable for the largest sizes of OM residues in line with the results of  
504 Masse et al. (2007) and Nunan et al. (2020). A better assimilation of biomass in the presence of small  
505 OM residues can be promoted by modifying the physiological parameters of fungal growth (Falconer et  
506 al., 2015). When increasing the carbon diffusion rates in the hyphae and lowering the associated

507 metabolic costs, the fungus develops an exploratory behavior and more easily finds the dispersed OM  
508 residues. These authors pointed out that bulk measurements of OM residues in soil samples are not  
509 sufficient to predict CO<sub>2</sub> production and that it is vital to describe spatial heterogeneity of soils at the  
510 microhabitat scale. They also advocated that macroscopic models should abandon the linear description  
511 of the response of soil microorganisms to nutrients on the basis of the bulk concentration of nutrients  
512 (Falconer et al., 2015).

513

#### 514 **2.4.2 Role of water saturation**

515 It has been long evinced that bacterial respiration depends on soil water saturation (e.g., Skopp et al.,  
516 1990). Water content, as well as the geometry and connectivity of pores control nutrient diffusion, soil  
517 aeration and accessibility of nutrients to bacteria. In agreement with experimental results, OM  
518 decomposition decreases in modelling scenarios involving decreasing water saturation levels (e.g.,  
519 Borer et al., 2019; Monga et al., 2008; Vogel et al., 2015; Yan et al., 2016). This effect is enhanced in  
520 the case of a heterogeneous distribution of OM residues. When OM is placed in large pores, the  
521 decomposition decreases when soil becomes drier because the large pores are first emptied of water and  
522 become isolated and are not accessible to bacteria (Monga et al., 2008). This is in line with the  
523 experimental results of Dechesne et al. (2010) where the decrease of substrate mineralization under  
524 heterogeneous distribution of bacteria accentuated with the decrease of matric potentials (from -1 kPa  
525 to -50 kPa).

526 Calibrating their microscale model on the growth of six bacterial strains in sand under saturated  
527 conditions, Monga et al. (2014) obtained longer lag times for respiration rates under drier conditions,  
528 compared to experimental data. This suggests that their micromodel underestimates the diffusion of  
529 fructose. One hypothesis put forward by the authors is an overestimation of the fragmentation of the  
530 liquid phase as wetting films are not considered in their morphological approach of pore space  
531 description. The fact that pores smaller than the resolution of the tomographic images (in this case 5  
532 µm) are ignored could also explain lower OM decomposition rates. When considering water films  
533 preserving connectivity for water saturation of 50 % in soil microaggregates, Zech et al. (2022)  
534 observed no difference in the total OM consumption and CO<sub>2</sub> production compared to the saturated  
535 case. However, differences arise locally with the onset of hot-spots of microbial activity depending on  
536 the geodesic distance of bacteria to OM source.

537 Other modelling scenarios have shown contrasting impact of water saturation on decomposition  
538 rates of soluble OM (Vogel et al., 2015; Mbé et al., 2021). This is related to the spatial accessibility of  
539 trophic resource to the decomposers, and to the amount of OM. Increase or decrease of fructose  
540 degradation are found when water saturation decreases (Vogel et al., 2015). Degradation decreases  
541 when bacterial colonies are located far from the initial fructose pulse and experience limiting diffusion  
542 conditions. However, when accessibility is optimal, degradation increases for low water saturation. In  
543 this latter case, the increase of fructose concentration in the remaining liquid phase stimulates bacterial  
544 growth. This stimulation can be so high that one bacterial spot can be as efficient in consuming DOC  
545 than ten of them (Vogel et al., 2015). In the case of homogeneous distribution of bacteria and DOC  
546 (Mbé et al., 2021), mineralization always increases, although to a small extent, when water saturation  
547 decreases. This effect is less pronounced in soil with higher bulk density, suggesting that the increase of  
548 DOC concentration in the remaining liquid phase explains this trend (Mbé et al. 2021). When the  
549 distribution of bacteria is aggregated in a small region, the amount of produced CO<sub>2</sub> is not anymore  
550 ranked according to water saturation, suggesting that stimulation of biomass growth by higher DOC  
551 concentrations can surpass diffusion constraints.

552 A heterogeneous microscale distribution of water-saturated regions in soils affects the intensity and  
553 location of reactive hotspots. Considering only aerobic respiration, Yan et al., (2018) showed how a  
554 balance between OM accessibility and O<sub>2</sub> diffusion can drive microbial respiration. Hotspots of OM  
555 decomposition are simulated under high water saturation conditions, which promotes OM  
556 bioavailability, whereas hotspots nearly disappear when water saturation further increases because this  
557 limits the gaseous diffusion of O<sub>2</sub>.

558 Most of the reported modelling studies have dealt with different water saturations but have ignored  
559 water advection and its complex role in influencing microbial response. In modelling scenarios  
560 describing an idealized straight pore and water saturated conditions, Schmidt et al. (2018) showed that  
561 in the presence of water flow, the aggregation of bacterial colonies can lead to a significant reduction in  
562 degradation rates. When bacteria are gathered in spots, they do not have the same access to the  
563 substrate as when they are distributed homogeneously along the pore. Consequently, due to advection,  
564 part of the substrate is evacuated from the pore without having been consumed. In a more complex  
565 description of soil architecture, Gharasoo et al. (2012) observed that an increase in the heterogeneity of  
566 the pore-size distribution leads to a decrease of substrate bioavailability because it increases

567 preferential flow paths. However, in their scenarios, heterogeneous distributions of biomass have a  
568 minor effect on substrate availability in the case of homogeneous pore-size distributions.

569

### 570 **2.4.3 Role of ecological interactions**

571 The role of ecological interactions combined with environmental conditions at the microhabitat  
572 scale is complex. Using an implicit description of soil architecture, Kaiser et al. (2014) showed how the  
573 spatio-temporal dynamics of interacting functional groups can alleviate microbial N limitation in the  
574 decomposition of litter of low C:N ratios. Ecological interactions can also maintain the rates of OM  
575 decomposition in the case of low spatial accessibility to nutrients . For instance, Portell et al. (2018)  
576 found unchanged overall carbon turnover for random or aggregated spatial distributions of OM, and  
577 Pagel et al. (2020) found that only a strong spatial clustering of decomposer communities can reduce  
578 the rate of decomposition of carbon compounds. In both studies three functional groups defined  
579 according to their capacity to consume the resources are considered. Redundancy of the three  
580 functional groups is suggested to compensate to some extent the diffusion limitations of nutrients  
581 (Pagel et al., 2020). However, when the diffusion limitations are too severe, compensation cannot be  
582 achieved.

583 The modelling scenarios of Nunan et al. (2020) explore different acquisition strategies of the  
584 resources ranging from generalists (bacterial taxa can consume the same resources) to specialists  
585 (bacterial taxa can consume only one resource), In the absence of functional redundancy (specialists),  
586 the proportion of resources consumed is increased when bacterial diversity increases, i.e., more taxa  
587 with fewer individuals consume more than few taxa with a higher number of individuals (Nunan et al.,  
588 2020). The aggregation of the resources increases only the variability of the consumption. When up to  
589 ten different resources are submitted to different acquisition strategies (generalists and/or specialists),  
590 the aggregation of OM gives a competitive advantage on generalists over specialists and the resource is  
591 more consumed (Nunan et al., 2020). There is a higher probability of co-location of generalist bacterial  
592 cells on one of the resources they can consume than for specialists. In these modelling scenarios, soil  
593 architecture is not described explicitly, and circular patches of OM are randomly distributed within a  
594 2D space, following the approach of Masse et al. (2007). A different picture emerges in scenarios where  
595 specialists are given an advantage on getting their food. In this microscale model, bacteria are singular  
596 spots and acquire resource within a disc whose radius can be modified (Nunan et al., 2020). When

597 increasing the size of the area where specialists can take up the resource, a disadvantage for generalists  
598 compared to specialists is found and leads to an overall low resource consumption.

599 A different result can be obtained, namely a decrease of OM decomposition, when bacterial diversity  
600 is high (Evans et al., 2016; Folse & Allison, 2012; Kaiser et al., 2015). In this case, ecological  
601 interactions are based on complementary resources acquisition in communities of producers and  
602 cheaters. When diffusion limitations are high, nutrient enzymatic depolymerization is increased in the  
603 presence of competitive interactions between different types of bacteria, from enzyme-producers to  
604 cheaters (Folse & Allison, 2012). Low diffusion limits the development of cheaters that rely on enzyme  
605 diffusion to survive. By contrast, in high diffusion situations, biodiversity is increased and the cheaters  
606 and coalitions of intermediate types in competition with the generalist producers reduce enzyme  
607 production and thus nutrient depolymerization (Folse & Allison, 2012). In the modelling scenarios of  
608 Kaiser et al. (2015), the decay rates of litter can be reduced by up to 90% in the presence of cheaters,  
609 depending on their maximum growth rate. This effect is further enhanced when ecological interactions  
610 are combined with variable water content as simulated in dry-rewetting cycles by Evans et al. (2016).  
611 During drought, a critical limitation by diffusion can locally create hotspots of dissolved OM due to the  
612 continuous enzymatic depolymerization. During re-wetting, diffusion of soluble compounds is  
613 increased and this additional amount of available OM triggers high increase of CO<sub>2</sub> production (e.g.,  
614 Barnard et al., 2020). This effect, known as the Birch effect, is dampened in presence of cheaters  
615 (Evans et al., 2016). Whereas cheaters are sensitive to drought, they out-compete enzyme-producers  
616 under rewetting. The fast response of cheaters when diffusion limitations are relieved upon rewetting,  
617 confers them an advantage over the producers and leads to an overall decrease of OM decomposition.

618

## 619 **2.5 Summary of main insights**

620 The many modelling scenarios investigated and the sometimes contradictory results obtained show  
621 the complexity arising from processes interacting at the microbial habitats. However, if we summarize  
622 these results in the light of the role of OM spatial accessibility to microorganisms, tendencies can be  
623 found (Table 1). In general, when spatial accessibility is optimal, it promotes SOM decomposition, CO<sub>2</sub>  
624 production and fungal expansion whereas soil biodiversity is reduced. Opposite results are found in the  
625 case of a low OM spatial accessibility. We could not extract clear trends for the bacterial spatial  
626 organization. However, we identified several parameters or processes that control the strength of these

627 microbial activities. These factors can relieve constraints imposed by low OM spatial accessibility and  
 628 reframe microbial activity to some extent (Table 1).

629

630 **Table 1:** Main effects of optimal and low OM spatial accessibility on microscale model outputs and main  
 631 sensible parameters and processes controlling or modifying (indicated in this case by blue symbols in  
 632 parentheses) these effects.

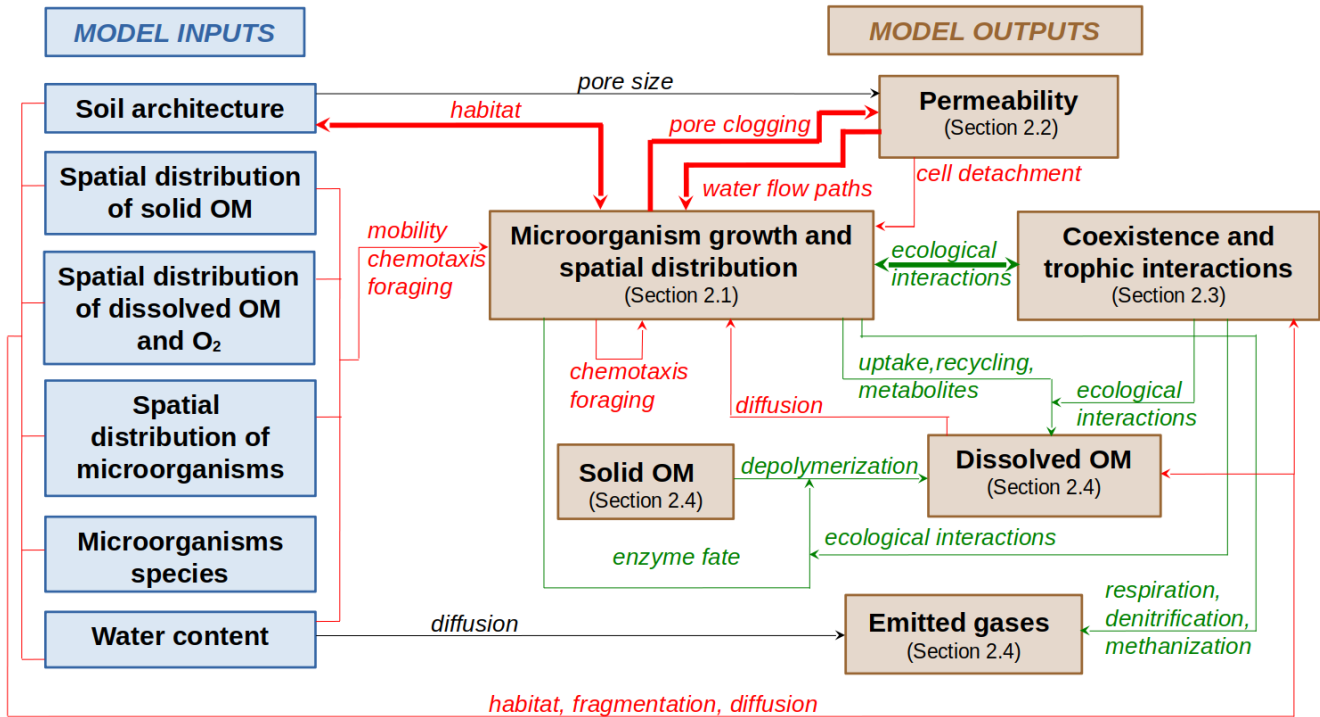
	optimal OM spatial accessibility	low OM spatial accessibility
Bacterial spatial organization	+/-	+/-
Fungal expansion	+	- (+)
Bacterial biodiversity	-	++ (+)
OM decomposition	++	-- (-)
CO2 production	++	-- (-)
Sensible parameters or processes	Maximum bacterial growth rate Enzyme production rate Ecological interactions Fungal biomass recycling	High bacterial growth rate High fungal biomass recycling Ecological interactions Chemotactic behaviour

### 636 3. Disentangling the role of soil architecture and microbial dynamics

637 In microscale models, one can decouple the respective roles of soil architecture and microbial  
 638 dynamics on soil functions by considering interactions at the microscopic scale and feedback loops, as  
 639 illustrated in Figure 3, which emphasizes the main links between the inputs and outputs of the models.  
 640 We can classify model inputs into six groups of different nature: 1) soil architecture, which describes  
 641 the spatial arrangement of soil particles, the geometry of pores and pore-solid interfaces; 2) water  
 642 content, which describes the amount of water and the distribution of air-water interfaces within the  
 643 pores; 3) the initial spatial distribution of solid OM; 4) the initial spatial distribution of dissolved  
 644 chemical species (including OM, O<sub>2</sub>, enzymes); 5) the initial spatial distribution of microbes, either in  
 645 suspension in the water phase and/or attached to the pore-solid interfaces (for bacteria), and in the air-  
 646 filled pore space (in the case of fungi); and 6) the initial species. The first five inputs are directly  
 647 related to the spatial accessibility of trophic resources to microbes. The six outputs are those reported in  
 648 the previous sections. Table S1 lists each reported microscale model according to this classification.

649 System properties or processes that directly influence spatial accessibility of the trophic resources to  
 650 microbes are displayed by red arrows. The green arrows correspond to ecological interactions and  
 651 processes that control the efficiency of microbes to depolymerize and uptake OM, emit gases and grow.

652 The black arrows correspond to other system properties or processes not linked to spatial accessibility  
 653 or microbial dynamics. Feedback loops are displayed by thick arrows in Figure 3.  
 654



655 **Figure 3:** Schematic overview of the main inputs and outputs of microscale models highlighting the spatial  
 656 and ecological interactions at the microhabitat scale. Red arrows correspond to interactions between inputs and  
 657 outputs that control spatial accessibility of the trophic resource to microbes. These links are associated to system  
 658 properties and processes. Green arrows correspond to the links that control the efficiency of microbes to  
 659 depolymerize and uptake OM and to emit gases. These links are associated to processes. Thick red and green  
 660 arrows correspond to feedback loops linked to spatial accessibility and ecological interactions respectively.  
 661 Black arrows correspond to other links that don't control spatial accessibility or efficiency of microbial activity.  
 662

663 From Figure 3, it can be seen that, in microscale models, soil architecture provides an initial stage of  
 664 spatial accessibility and promotes interactions between the actors of OM decomposition (red arrows  
 665 between inputs). This accessibility is a key factor explaining most of the model outputs, from a direct  
 666 influence on hydraulic properties (pore size, black arrow) to indirect influences on the decomposition  
 667 of OM, emission of gases and soil biodiversity maintenance through its role in shaping the spatial  
 668 accessibility (red arrows between inputs and outputs). The temporal dynamics of most of the outputs  
 669 (the spatial distribution of microbial colonies, dissolved OM, soil hydraulic properties, soil

670 biodiversity) makes spatial accessibility a highly dynamic variable and contributes thus to feedback  
671 loops. We identified three feedback loops: (i) soil architecture provides an habitat for microorganisms  
672 growth and distribution and in turn microorganisms modify soil architecture (through fungal  
673 enmeshment, aggregation) (thick red arrow); (ii) water flow paths can alter the spatial distribution of  
674 microorganisms which in turn can alter the pore geometry (until pore clogging) that modifies  
675 permeability and water flow paths (two thick red arrows); (iii) biodiversity creates ecological  
676 interactions that have an impact on the microorganism growth and distribution which in turn can  
677 modify the biodiversity by sustaining or extinguishing species (thick green arrow). Finally, microbial  
678 dynamics and ecological interactions can relieve constraints imposed by low spatial accessibility (green  
679 arrows).

680       Microscale models are thus a useful tool to help disentangle these complex interactions between soil  
681 architecture and microbial dynamics and rank their contributions. In a few studies they have been used  
682 to quantify and rank these complex interactions. In a sensitivity analysis performed on a factorial  
683 design where geometry of the pore space, water saturation, spatial distribution of bacteria and  
684 physiological trait (bacterial dormancy) are the factors, Vogel et al. (2015) found, for their modelling  
685 scenarios, that bacterial spatial distribution alone explains about 30% of the total variance of fructose  
686 decrease. About half of the variance of fructose decrease is explained by two-factor interactions  
687 between water saturation and bacterial spatial distribution, between geometry of pore space and water  
688 saturation, and between geometry of pore space and bacterial spatial distribution. Interestingly, under  
689 optimal accessibility, physiological parameters can generate greater variability in fructose decrease,  
690 CO<sub>2</sub> production and biomass growth (Vogel et al., 2018). When accessibility is low, the consumption of  
691 fructose remains very limited regardless of the efficiency of microbial uptake. This is in line with Pagel  
692 et al. (2020) who reported that maximum growth rate can have a higher influence than the spatial  
693 heterogeneity of the microbes on the resource consumption. In another sensitivity analysis of a fungal  
694 growth microscale model, Cazelles et al. (2013) also showed that parameters related to biomass  
695 recycling processes, and in particular the biomass yield efficiency, strongly impact total biomass and  
696 respiration. These parameter sensitivities are further dependent on the microenvironment contexts. For  
697 example, variability in spatial colonization of pores by a fungus is affected by the parameter describing  
698 immobilisation of mobile biomass in the mycelium in scenarios where the carbon resource is  
699 homogeneously distributed in the pore space. By contrast, it is the parameter describing the reverse



700 process, mobilization of the insulated biomass, that is sensitive in scenarios where carbon resource is  
701 initially co-located with the fungal inoculum (Cazelles et al., 2013).

702 Vogel et al. (2018) pointed out that measuring the time evolution of bulk DOC concentration is the  
703 best proxy to identify the role of soil architecture and micro-environments on microbial activity.  
704 Although easier to measure, the time evolution of CO<sub>2</sub> is less informative because CO<sub>2</sub> is a more  
705 integrative variable and its dynamics is also strongly influenced by the physiology of bacteria (Vogel et  
706 al., 2018).

707

## 708 **4. Discussion**

### 709 **4.1 Assessment of microscale models**

710 Most of the reported microscale models play with “what-if” scenarios to understand the interactions  
711 between the actors that control the soil microbial activity. Then, the trends observed are generally  
712 compared to experimental findings. The majority of studies that have tried to reproduce experimental  
713 conditions consider idealized geometries such as micromodels (e.g., Borer et al., 2018, 2019; Centler et  
714 al., 2011), packs of spherical grains (e.g., Gharasoo et al., 2012; Peszynska et al., 2016) and in a few  
715 cases repacked soils (e.g., Babey et al., 2017, Monga et al., 2014). Assessment of microscale models on  
716 experimental microfluidic devices, as advocated by Smercina et al. (2021), appears promising since  
717 biodiversity and the movement of microbes can be easily controlled and monitored (e.g., Long &  
718 Hilpert, 2008). For example, Borer et al. (2019) were able to reconcile contradictory results between  
719 their microscale model and experiments carried out on microfluidic devices by introducing more  
720 complex metabolic pathways in their biological module.

721 Due to the simplification of the biodiversity contained in microscale models and the still  
722 unreachable description of the whole span of pore size of soil architecture, assessing microscale models  
723 against experiments in intact soil samples seems unrealistic. Comparison of microscale models to  
724 controlled experiments in soils that have attempted to simplify biodiversity also faces a number of  
725 difficulties. Sterilization of soils and inoculation of specific micro-organisms have unwanted  
726 consequences, such as an unrealistic increase of necromass. Inoculation of the targeted species also  
727 poses the question on where to localize the microorganisms in the pores (e.g., Juarez et al., 2013;  
728 Pinheiro et al. 2015). Maintaining sterile conditions throughout incubation experiments also makes the  
729 experimental protocols considerably more cumbersome. Several attempts have considered instead the  
730 injection of labeled dissolved OM into different pore sizes to activate microorganisms located in these

731 pores (e.g., Ruamps et al., 2011; Kravchenko et al., 2020). However, as pointed out by Baveye et al.  
732 (2018) there is still a lack of experimental data to better characterize soil heterogeneity at the  
733 microscale habitat and this also contributes to hindering attempts to accurately assess microscale  
734 models.

735

#### 736 **4.2 How to upscale the information given by microscale models**

737 Another difficult challenge is how to translate the knowledge gained on interactions at the  
738 microscopic scale into larger scales (König et al., 2020). Upscaling differential equations of reactive  
739 transport including non-linear reaction rates, such as Monod-type reaction rates, is complex because it  
740 leads to a concentration-dependent transition between reaction-limited and diffusion-limited regimes  
741 which is not observed for first-order reaction rates (Heße et al., 2009). This results in an upscaling  
742 behavior depending on the substrate concentration. In a simple pore geometry, Heße et al., (2009)  
743 succeeded in finding two concentration-independent effective parameters in situations of biomass  
744 continuously covering pore walls. These effective parameters were successfully applied to  
745 heterogeneous bacterial colonies distribution within a straight pore (Schmidt et al., 2018). However, it  
746 is expected that additional scaling factors that are functionals of pore geometry should be considered to  
747 improve the upscaled rate estimates in complex soil architecture (Jung & Meile, 2019). Chakrawal et  
748 al. (2020) advocated for the use of the scale transition theory, which upscales population dynamic  
749 functions (such as Monod dynamics) instead of the partial differential equations of fluxes, as performed  
750 in predator-prey ecology models (e.g., Bergström et al., 2006). In this theory, the spatial heterogeneity  
751 of substrate and microorganisms at the microscale is considered by keeping the second-order spatial  
752 moments when spatially averaging the functions. However analytical expression of these second-order  
753 moments have yet to be developed for non-linear reaction rates. Using another approach, Ebrahimi and  
754 Or (2016, 2017, 2018) proposed an upscaling procedure to compute the flux of biogeochemical gases at  
755 the soil profile scale by using a microscale model that calculates the gases produced in single  
756 aggregates of different sizes. Then, the fluxes are summed up to represent those resulting from an  
757 assembly of soil aggregates. However, this approach assumes that the aggregates are surrounded by air-  
758 filled pores which is not necessarily the case (Baveye et al., 2022; Vogel et al., 2021; Kravchenko et al.,  
759 2019).

760 Alternatively, microscale models can be used to search for a suitable formulation of the effective  
761 reaction rate in macroscopic soil carbon models or to improve multiplicative functions used to weight

762 the effective reaction rate. For instance, Wang & Allison (2019) found that enzymatic degradation rates  
763 based on the equilibrium chemistry approximation (ECA, Tang & Riley, 2013), which is a more general  
764 formulation of “reverse” and “forward” Michaelis-Menten kinetics, could be used to fit outputs from  
765 the DEMENT microscale model (Allison, 2012), which uses “forward” Michaelis-Menten kinetics.  
766 Ruiz et al. (2020) could fit a simple macroscopic nitrogen model to predictions of a microscale model  
767 carried out in complex soil architecture provided that two parameters linked to surface to volume ratios  
768 of fertilizer pellets and soil surfaces respectively are considered in the formulation of the dissolved  
769 organic nitrogen rates. These results are in line with those of Garnier et al. (2008) and Iqbal et al.  
770 (2014) who could fit the macroscopic OM decomposition model CANTIS (Garnier et al., 2003) with  
771 measured data of incubation of plant residues, provided that a parameter linearly linked with the  
772 specific surface of residues is included in the effective decomposition rate. Thus, rate modifiers that  
773 take into account the role of spatial accessibility of OM to the soil decomposers could be found.  
774 Indeed, by ignoring spatial information, macroscopic models of OM turnover assume optimal spatial  
775 accessibility and may overestimate CO<sub>2</sub> production.

776 Rather than mathematically upscaling to larger spatial scales, a few modelling studies have  
777 attempted to finding spatial descriptors of soil architecture that could encompass these microscopic  
778 interactions and statistically correlate with the model outputs. Most of these descriptors are based on  
779 the spatial accessibility of microbes to the trophic resources. Wang & Or (2012) proposed a bacterial  
780 coexistence index equal to the ratio of a characteristic distance traversed by a bacterial cell generation  
781 to the effective radius of water clusters. This index aims to quantify the role of soil architecture and  
782 hydration status of pores on the coexistence of two competitive species. Portell et al. (2018) calculated  
783 the geodesic distance from bacterial colonies to OM residues and compared them to growth of these  
784 colonies. They showed that none of the colonies are able to develop for a geodesic distance greater than  
785 around 5 mm, which is consistent with experimental data (Gaillard et al., 1999; Védère et al., 2020).  
786 The most active microbial habitats are those with the shortest geodesic distance, however some habitats  
787 do not develop although they are at a short geodesic distance from the residues. This suggests that other  
788 variables such as the local soluble carbon concentration reaching the microhabitats may play a role.  
789 This was considered in the accessibility coefficient of Mbé et al. (2021), which is calculated as the  
790 average of the shortest geodesic distance between bacterial colonies and OM residues, multiplied by  
791 the amount of OM in each residue. Satisfactory statistical correlations (linear regression coefficient R<sup>2</sup>  
792 of 0.7) between simulated CO<sub>2</sub> and this microscale descriptor is found for different modelling

793 scenarios. Although these results are encouraging, these latter two descriptors do not consider other  
794 processes such as the protection of OM by mineral-associations (e.g., Basile-Doelsch et al., 2020), the  
795 translocation of carbon by fungi that can dynamically alter the accessibility of OM in intact soils (e.g.,  
796 Boswell et al., 2003, 2007; Védère et al., 2020; Vidal et al., 2021), the spatial invasion of fungi and to a  
797 lesser extent the motility of bacteria by chemotaxis or using fungal highways (e.g., Banitz et al., 2011).  
798 Banitz et al. (2016) found that the combination of two metrics describing the spatial configuration of  
799 fungal highways for bacteria was best suited to explain the biodegradation of glucose. The advantage of  
800 spatial descriptors based on accessibility of OM is that they can be calculated in soil CT images,  
801 provided that accurate segmentation of air, water and organic matter phases are achieved (e.g., Rawlins  
802 et al., 2016; Ortega-Ramirez et al., 2021; Rohe et al., 2021). Development of complementary 2D  
803 imaging tools such as microscopy and nanoSIMS which provide spatial distribution of chemicals and  
804 microorganisms (e.g., Eickhorst & Tippkötter, 2008; Vidal et al., 2021) and whose integration with CT  
805 images has begun (Hapca et al. 2011; Schlüter et al., 2019) will certainly help to give accurate  
806 information on the relative distributions of OM and microorganisms.

807

### 808 **4.3 Overall limitations and future directions of microscale modelling**

809 Describing spatialized microbial activity in 3D and at the microhabitat scale asks for intense  
810 computational resources. Obviously, microscale models are not designed to describe soil biodiversity in  
811 detailing the many species and complex food webs, which should be better left for ecological models.  
812 Nonetheless, the latter may identify main functional groups to be included in microscale models.

813 We advocate for introducing a dynamical soil architecture in microscale models. Environmental  
814 factors such as drying-rewetting cycles and feedbacks of microbial activity on modifying transport  
815 pathways and microbial habitats change the spatial OM accessibility. Microscale models would be  
816 good candidates to test the hypotheses explaining the still poorly understood Birch effect (Schimel,  
817 2018) that can result in large amounts of emitted CO<sub>2</sub> (e.g., Barnard et al., 2020). Incentive works are  
818 those of Ebrahimi & Or (2018), Evans et al. (2016), Šťovíček et al., (2017), Wang & Or (2013) and  
819 Zech et al. (2022) who evolved water content at the grid nodes to simulate drying-rewetting cycles. In  
820 addition, based on experimental data obtained with X-ray CT imaging tools such as the ones by  
821 Bottinelli et al. (2016) one could draw statistical rules to modify the size and connectivity of pores.

822 Another research gap is the role of meso and macro fauna that, to our knowledge, has been ignored  
823 in microscale modelling. Worms (e.g., earthworms, enchytraeids) play an important role in soil carbon

824 and nitrogen mineralization. Their casts are hotspots for microbial activity, and they modify the pore  
825 space morphology through their burrowing activity thereby impacting gas exchanges and transfer in the  
826 active microsites. As a result, enhanced CO<sub>2</sub> and N<sub>2</sub>O emissions were reported in the presence of  
827 worms (e.g., Lubbers et al., 2010; Porre et al., 2016). Including experimental imaging data of burrow  
828 systems such as enchytraeids in microscale models would be a good start, as their size fits the  
829 microscale models better than earthworm.

830 We also advocate for including rhizosphere in microscale models. Indeed, most of the reported  
831 studies have dealt with detritosphere. However, rhizosphere constitutes hotspots of soil microbial  
832 activity and rhizodeposition has a role in priming effect and soil aggregation (e.g., Baumert et al.,  
833 2018). Current advances in modelling and experimental methods offer now opportunities to quantify  
834 the rhizosphere at microscopic scales and advance new insights how these microscopic processes  
835 impact across scales, and current challenges in the rhizosphere (Schnepf et al., 2022). Microscale  
836 models could help in quantifying the respective role of detritosphere and rhizosphere in SOM  
837 decomposition and greenhouse gases production. To do so, microscale models could benefit from 3D  
838 models of root water and nutrients uptake that include soil-root interactions and high-performance  
839 imaging tools that reveal root architecture (e.g., Keyes et al., 2013) .

840

## 841 **5. Conclusions**

842 Microscale models provide valuable “what-if” scenarios to test hypotheses about the role of soil  
843 architecture and microbial dynamics to explain non-linear responses of soil microorganisms. The  
844 reported modelling scenarios highlight how microbial activity relies on a balance between the physical  
845 and biological processes taking place in the complex soil architecture and reveal threshold effects. They  
846 confirm that soil architecture does matter. For example, it contributes to the emergence of a spatial  
847 organization of the microbial communities which in turn can modify significantly soil OM  
848 decomposition and soil gaseous emissions. They highlight the role of spatial accessibility of trophic  
849 resources to microbes, which when combined with ecological interactions, can shape different pictures  
850 regarding the amount of OM decomposed in soil. Indeed, microbial dynamics and ecological  
851 interactions can counterbalance limitations imposed by low spatial accessibility of OM to decomposers.  
852 When spatial accessibility is optimal, they become the major drivers of soil OM decomposition. Local  
853 accumulation of biomass can also alter hydraulic properties of soil and influence water flow field.  
854 Microscale models also demonstrate that using bulk measures such as bulk water content or bulk soil

855 density is clearly insufficient to predict soil microbial activity. An accurate description of both the soil  
856 microhabitats and microbial dynamics in models is thus crucial to understand soil functions.

857 Even though the assessment of microscale models is still limited, due to a scarcity of relevant  
858 experimental data on soils, these models are useful tools to search for spatial descriptors of the soil  
859 micro-environments explaining soil microbial activity. Another key function of these microscale  
860 models at this early stage is to guide experimentation by generating new and testable hypotheses based  
861 upon our current knowledge, which is encapsulated in the models. Modelling also helps to integrate  
862 new knowledge we gain from improved technology, which unravels novel information at  
863 microscopic/nano scales.

864

## 865 **6. Acknowledgment**

866 The research reported on in this article was supported by a grant from the French Agence Nationale  
867 de la Recherche to project Soil  $\mu$ -3D (ANR-15-CE01-0006). Additionally, WO and XP received  
868 support from the National Environment Research Council (NE/P014208/1 and NE/S004920/1). XP is  
869 currently a María Zambrano Fellow at the Public University of Navarra (UPNA) and acknowledges  
870 funding from the European Union - NextGenerationEU through the Spanish program "Ayuda para la  
871 Recualificación del Sistema Universitario Español".

872

## 873 **7. Data availability statement**

874 Data sharing is not applicable to this article as no new data were created or analyzed in this study.

875

## 876 **8. References**

- 877 Allison, S. D. (2005). Cheaters, diffusion and nutrients constrain decomposition by microbial enzymes  
878 in spatially structured environments. *Ecology Letters*, 8, 626–635. <https://doi.org/10.1111/j.1461-0248.2005.00756.x>  
879
- 880 Allison, S.D. (2012). A trait-based approach for modelling microbial litter decomposition. *Ecology*  
881 *Letters* 15, 1058–1070. doi:10.1111/j.1461-0248.2012.01807.x
- 882 Angers D.A., Recous S. (1997). Decomposition of wheat straw and rye residues as affected by particle  
883 size. *Plant and Soil* 189, 197-203. doi:<https://doi.org/10.1023/A:1004207219678>

884 Aravena J.E., Berli M., Ruiz S., Suarez F., Ghezzehei T.A., Tyler S.W. (2014). Quantifying coupled  
885 deformation and water flow in the rhizosphere using X-ray microtomography and numerical  
886 simulations. *Plant Soil* 376, 95–110. doi:10.1007/s11104-013-1946-z

887 Babey, T., Vieublé-Gonod, L., Rapaport, A., Pinheiro, M., Garnier, P. & de Dreuzy, J.R. (2017).  
888 Spatiotemporal simulations of 2,4-D pesticide degradation by microorganisms in 3D soil-core  
889 experiments. *Ecological Modelling* 344, 48-61. DOI: 10.1016/j.ecolmodel.2016.11.006

890 Bailey D.J., Otten W., Gillican C.A. (2000). Saprotrophic invasion by the soil-borne fungal plant  
891 pathogen *Rhizoctonia solani* and percolation thresholds. *New Phytologist* 146, 535-544.  
892 doi:10.1046/j.1469-8137.2000.00660.x

893 Banitz, T., Fetzer, I., Johst, K., Wick, L. Y., Harms, H., & Frank, K. (2011). Assessing biodegradation  
894 benefits from dispersal networks. *Ecological Modelling*, 222, 2552–2560.  
895 <https://doi.org/10.1016/j.ecolmodel.2010.07.005>

896 Banitz, T., Frank, K., Wick, L. Y., Harms, H., & Johst, K. (2016). Spatial metrics as indicators of  
897 biodegradation benefits from bacterial dispersal networks. *Ecological Indicators*, 60, 54–63.  
898 <https://doi.org/10.1016/j.ecolind.2015.06.021>

899 Barnard R.L., Blazewicz S.J., Firestone M.K. (2020) Rewetting of soil: Revisiting the origin of soil  
900 CO<sub>2</sub> emissions. *Soil Biology and Biochemistry* 147, 107819. doi:10.1016/j.soilbio.2020.107819

901 Basile-Doelsch I., Balesdent J., Pellerin S. (2020). Reviews and syntheses: The mechanisms underlying  
902 carbon storage in soil. *Biogeosciences* 17, 5223-5242. doi:10.5194/bg-17-5223-2020

903 Baumert VL, Vasilyeva NA, Vladimirov AA, Meier IC, Kögel-Knabner I and Mueller CW (2018).  
904 Root Exudates Induce Soil Macroaggregation Facilitated by Fungi in Subsoil. *Frontiers in*  
905 *Environmental Science* 6, 140. doi: 10.3389/fenvs.2018.00140

906 Baveye P.C. (2020). “Soil biofilms”: Misleading description of the spatial distribution of microbial  
907 biomass in soils. *Soil Ecology Letters* 2, 2-5. doi:10.1007/s42832-020-0024-8

908 Baveye, P. C., Balseiro-Romero, M., Bottinelli, N., Briones, M., Capowiez, Y., Garnier, P., Kravchenko,  
909 A., Otten, W., Pot, V., Schlüter, S., Vogel, H.J., (2022). Lessons from a landmark 1991 article on soil  
910 structure: distinct precedence of non-destructive assessment and benefits of fresh perspectives in soil  
911 research. *Soil Research*. In press. doi: 10.1071/SR21268

912 Baveye, P. C., Berthelin, J., & Munch, J. C. (2016). Too much or not enough: reflection on two  
913 contrasting perspectives on soil biodiversity. *Soil Biology and Biochemistry*, 103, 320-326. doi:  
914 10...1016/j.soilbio.2016.09.008

915 Baveye P.C., Otten W., Kravchenko A., Balseiro-Romero M., Beckers E., Chalhoub M., Darnault C.,  
916 Eickhorst T., Garnier P., Hapca S., Kiranyaz S., Monga O., Mueller C.W., Nunan N., Pot V., Schlüter  
917 S., Schmidt H., Vogel H.J. (2018). Emergent properties of microbial activity in heterogeneous soil  
918 microenvironments: Different research approaches are slowly converging, yet major challenges  
919 remain. *Frontiers in Microbiology* 9, 1929. doi: 10.3389/fmicb.2018.01929

920 Bending G.D., Turner M.K. (1999). Interaction of biochemical quality and particle size of crop residues  
921 and its effect on the microbial biomass and nitrogen dynamics following incorporation into soil.  
922 *Biology and Fertility of Soils* 29, 319-327. doi:10.1007/s003740050559

923 Bergström, U., Englund, G., and Leonardsson, K. (2006). Plugging space into predator-prey models: an  
924 empirical approach., *The American Naturalist* 167, 246–259. doi:10.1086/499372, 2006.

925 Borer B., Ataman M., Hatzimanikatis V., Or D. (2019). Modeling metabolic networks of individual  
926 bacterial agents in heterogeneous and dynamic soil habitats (IndiMeSH). *PLoS Computational*  
927 *Biology* 15, e1007127. doi:10.1371/10.1371/journal.pcbi.1007127

928 Borer B., Tecon R., Or D. (2018). Spatial organization of bacterial populations in response to oxygen  
929 and carbon counter-gradients in pore networks. *Nature communications* 9, 769. doi:10.1038/s41467-  
930 018-03187-y

931 Boswell G.P. (2008). Modelling mycelial networks in structured environments. *Mycological Research*  
932 112, 1015-1025. doi:10.1016/j.mycres.2008.02.006

933 Boswell, G., Jacobs, H., Davidson, F. A., Gadd, G. M., & Ritz, K. (2003). Growth and function of  
934 fungal mycelia in heterogeneous environments. *Bulletin of Mathematical Biology*, 65, 447–477.  
935 [https://doi.org/10.1016/S0092-8240\(03\)00003-X](https://doi.org/10.1016/S0092-8240(03)00003-X)

936 Boswell, G. P., Jacobs, H., Ritz, K., Gadd, G. M., & Davidson, F. A. (2007). The development of fungal  
937 networks in complex environments. *Bulletin of Mathematical Biology*, 69, 605–634.  
938 doi:10.1007/s11538-005-9056-6

939 Bottinelli N, Zhou H, Boivin P, Zhang ZB, Jouquet P, Hartmann C, Peng X (2016). Macropores  
940 generated during shrinkage in two paddy soils using X-ray micro-computed tomography. *Geoderma*  
941 265, 78-86. doi:10.1016/j.geoderma.2015.11.011

942 Cazelles K., Otten W., Baveye P.C., Falconer R.E. (2013). Soil fungal dynamics: Parameterisation and  
943 sensitivity analysis of modelled physiological processes, soil architecture and carbon distribution.  
944 *Ecological Modelling* 248, 165-173. doi:10.1016/j.ecolmodel.2012.08.008



945 Centler , F., Fetzer, I., & Thullner, M. (2011). Modeling population patterns of chemotactic bacteria in  
946 homogeneous porous media. *Journal of Theoretical Biology*, 287, 82–91.  
947 <https://doi.org/10.1016/j.jtbi.2011.07.024>

948 Chakrawal A., Herrmann A.M., Koestel J., Jarsjö J., Nunan N., Kätterer T., Manzoni S. (2020).  
949 Dynamic upscaling of decomposition kinetics for carbon cycling models. *Geoscientific Model*  
950 *Development* 13, 1399-1429. doi:10.5194/gmd-13-1399-2020

951 Cook A.R., Otten W., Marion G., Gibson G., Gilligan C.A. (2007). Estimation of multiple transmission  
952 rates for epidemics in heterogeneous populations. *Proceedings of the National Academy of Sciences*  
953 104, 20392-7. doi:10.1073/pnas.0706461104

954 Crawford J.W., Deacon L., Grinev D., Harris J.A., Ritz K., Singh B.K., Young I. (2012). Microbial  
955 diversity affects self-organization of the soil –microbe system with consequences for function  
956 *Journal of the Royal Society of Interface* 9, 1302–1310. doi:10.1098/rsif.2011.0679

957 Dechesne A., Owsianiak W., Bazire A., Grundmann G.L., Binning P.J., Smets B.F. (2010).  
958 Biodegradation in a Partially Saturated Sand Matrix : Compounding Effects of Water Content,  
959 Bacterial Spatial Distribution, and Motility. *Environmental Science & Technology* 44, 2386-2392.  
960 doi:10.1021/es902760y.

961 Ebrahimi A., Or D. (2014). Microbial dispersal in unsaturated porous media: Characteristics of motile  
962 bacterial cell motions in unsaturated angular pore networks. *Water Resources Research* 50, 7406-  
963 7429. doi:10.1002/2014WR015897

964 Ebrahimi A.N., Or D. (2015). Hydration and diffusion processes shape microbial community  
965 organization and function in model soil aggregates. *Water Resources Research* 51, 9804-9827.  
966 doi:10.1002/2015WR017565

967 Ebrahimi A., Or D. (2016). Microbial community dynamics in soil aggregates shape biogeochemical  
968 gas fluxes from soil profiles – upscaling an aggregate biophysical model. *Global Change Biology*  
969 22, 3141-3156. doi:10.1111/gcb.13345

970 Ebrahimi, A., & Or, D. (2017). Mechanistic modeling of microbial interactions at pore to profile scale  
971 resolve methane emission dynamics from permafrost soil. *Biogeosciences* 122, 1216–1238.  
972 doi:10.1002/2016JG003674

973 Ebrahimi, A., & Or, D. (2018). Dynamics of soil biogeochemical gas emissions shaped by remolded  
974 aggregate sizes and carbon configurations under hydration cycles. *Global Change Biology* 24, e378–  
975 e392. doi:10.1111/gcb.13938

976 Eickhorst, T., Tippkötter, R. (2008). Improved detection of soil microorganisms using fluorescence in  
977 situ hybridization (FISH) and catalyzed reporter deposition (CARD-FISH). *Soil Biology and*  
978 *Biochemistry*, 40, 1883–1891. doi:10.1016/j.soilbio.2008.03.024

979 Erktan A., Or D., Scheu S. (2020). The physical structure of soil: Determinant and consequence of  
980 trophic interactions. *Soil Biology and Biochemistry* 148, 107876. doi:10.1016/j.soilbio.2020.107876

981 Evans S., Dieckmann U., Franklin O., Kaiser C. (2016). Synergistic effects of diffusion and microbial  
982 physiology reproduce the Birch effect in a micro-scale model. *Soil Biology and Biochemistry* 93, 28-  
983 37. doi:10.1016/j.soilbio.2015.10.020

984 Falconer R.E., Bown J.K., White N.A., Crawford J.W. (2005). Biomass recycling and the origin of  
985 phenotype in fungal mycelia. *Proceedings of the Royal Society B* 272, 1727-1734.  
986 doi:10.1098/rspb.2005.3150

987 Falconer R.E., Battaia G., Schmidt S., Baveye P., Chenu C., Otten W. (2015). Microscale Heterogeneity  
988 Explains Experimental Variability and Non-Linearity in Soil Organic Matter Mineralisation. *PLOS*  
989 *One* 10, e0123774. doi:10.1371/journal.pone.0123774

990 Falconer R.E., Brown J.L., White N.A., Crawford J.W. (2007). Biomass recycling : a key to efficient  
991 foraging by fungal colonies. *Oikos* 116, 1558-1568. doi:10.1111/j.2007.0030-1299.15885.x

992 Falconer R.E., Bown J.L., White N.A., Crawford J.W. (2008). Modelling interactions in fungi. *Journal*  
993 *of the Royal Society Interface* 5, 603–615. doi:10.1098/rsif.2007.1210

994 Falconer R., Houston A.N., Otten W., Baveye P.C. (2012). Emergent Behavior of Soil Fungal  
995 Dynamics : Influence of Soil Architecture and Water Distribution. *Soil Science* 177, 111-119.  
996 doi:10.1097/SS.0b013e318241133a

997 Fierer N., Schimel J.P., Holden P.A. (2003). Influence of Drying-Rewetting Frequency on Soil  
998 Bacterial Community Structure. *Microb Ecol* 45, 63–71 doi:10.1007/s00248-002-1007-2

999 Flemming, H. C., Baveye, P., Neu, T. R., Stoodley, P., Szewzyk, U., Wingender, J., & Wuertz, S.  
1000 (2021). Who put the film in biofilm? The migration of a term from wastewater engineering to  
1001 medicine and beyond. *npj Biofilms and Microbiomes*, 7(1), 1-5. Doi: 10.1038/s41522-020-00183-3.

1002 Folse III H.J., Allison S.D. (2012). Cooperation, competition, and coalitions in enzyme-producing  
1003 microbes: Social evolution and nutrient depolymerisation rates. *Frontiers in Microbiology* 3, 338.  
1004 doi:10.3389/fmicb.2012.00338

1005 Franzluebbbers A.J. (1999). Microbial activity in response to water-filled pore space of variably eroded  
1006 southern Piedmont soils. *Applied Soil Ecology* 11, 91-101. doi:10.1016/S0929-1393(98)00128-0

1007 Gaillard, V., Chenu, C., Recous, S., Richard, G. (1999). Carbon, nitrogen and microbial gradients  
1008 induced by plant residues decomposing in soil. *European Journal of Soil Science* 50, 567–578.  
1009 doi:10.1046/J.1365-2389.1999.00266.X

1010 Garnier P., Cambier C., Bousso M., Masse D., Chenu C., Recous S. (2008). Modeling the influence of  
1011 soil-plant residue contact on carbon mineralization: Comparison of a compartmental approach and a  
1012 3D spatial approach. *Soil Biology and Biochemistry* 40, 2754-2761.  
1013 doi:10.1016/j.soilbio.2008.07.032

1014 Garnier P., Neel C., Aita C., Recous S., Lafolie F., Mary B. (2003). Modelling carbon and nitrogen  
1015 dynamics in soil with and without straw incorporation. *European Journal of Soil Science*, 54:555–  
1016 568. doi:10.1046/j.1365-2389.2003.00499.x

1017 Gharasoo M., Centler F., Fetzer I., Thullner M. (2014). How the chemotactic characteristics of bacteria  
1018 can determine their population patterns. *Soil Biology and Biochemistry* 69, 346-358.  
1019 doi:10.1016/j.soilbio.2013.11.019

1020 Gharasoo, M., Centler, F., Regnier, P., Harms, H., & Thullner, M. (2012). A reactive transport modeling  
1021 approach to simulate biogeochemical processes in pore structures with pore-scale heterogeneities.  
1022 *Environmental Modelling & Software*, 30, 102–114. doi:10.1016/j.envsoft.2011.10.010

1023 Graf von der Schulenburg D.A., Pintelon T.R.R., Picioreanu C., Van Loosdrecht M.C.M., Johns M.L.  
1024 (2009). Three-Dimensional Simulations of Biofilm Growth in Porous Media. *AIChE Journal* 55,  
1025 494-504. doi:10.1002/aic.11674

1026 Gras, A., M. Ginovart, J. Valls and P. C. Baveye (2011). Individual-based modelling of carbon and  
1027 nitrogen dynamics in soils: parameterization and sensitivity analysis of microbial components.  
1028 *Ecological Modelling* 222, 1998–2010. doi:10.1016/j.ecolmodel.2011.03.009

1029 Hapca, S. M., Wang, Z. X., Otten, W., Wilson, C., & Baveye, P. C.  
1030 (2011). Automated statistical method to align 2D chemical maps with 3D X-ray computed micro-  
1031 tomographic images of soils. *Geoderma*, 164(3–4), 146–154.  
1032 <https://doi.org/10.1016/j.geoderma.2011.05.018>

1033 Harris K., Young I.M., Gilligan C.A., Otten W., Ritz K. (2003). Effect of bulk density on the spatial  
1034 organisation of the fungus *Rhizobacteria solani* in soil. *FEMS Microbiology Ecology* 44, 45-56.  
1035 doi:10.1111/j.1574-6941.2003.tb01089.x

1036 Heße F., Radu F.A., Thullner M., Attinger S. (2009). Upscaling of the advection–diffusion–reaction  
1037 equation with Monod reaction. *Advances in Water Resources* 32, 1336–1351.  
1038 doi:10.1016/j.advwatres.2009.05.009

1039 Iqbal A., Garnier P., Lashermes G., Recous S. (2014). A new equation to simulate the contact between  
1040 soil and maize residues of different sizes during their decomposition. *Biology and Fertility of Soils*  
1041 (2014) 50:645–655. doi:10.1007/s00374-013-0876-5

1042 Juarez S. Nunan N., Duday A-C., Pouteau V., Chenu C. (2013). Soil carbon mineralisation responses to  
1043 alterations of microbial diversity and soil structure. *Biology and Fertility of Soils* 49, 939–948.  
1044 doi:10.1007/s00374-013-0784-8

1045 Jung H., Meile C. (2019). Upscaling of microbially driven first-order reactions in heterogeneous porous  
1046 media. *Journal of Contaminant Hydrology* 224, 103483. doi:/10.1016/j.jconhyd.2019.04.006

1047 Kaiser, C., Franklin, O., Dieckmann, U., & Richter, A. (2014). Microbial community dynamics  
1048 alleviate stoichiometric constraints during litter decay. *Ecology Letters*, 17, 680–690.  
1049 doi:10.1111/ele.12269

1050 Kaiser C., Franklin O., Richter A., Dieckmann U. (2015). Social dynamics within decomposer  
1051 communities lead to nitrogen retention and organic matter build-up in soils. *Nature Communications*  
1052 6:8960. doi: 10.1038/ncomms9960

1053 Kapellos G.E., Alexiou T.S., Payatakes A.C. (2007). Hierarchical simulator of biofilm growth and  
1054 dynamics in granular porous materials. *Advances in Water Resources* 30, 1648–1667.  
1055 doi:10.1016/j.advwatres.2006.05.030

1056 Keyes SD, Daly KR, Gostling NJ, Jones DL, Talboys P, Pinzer BR, Boardman R, Sinclair I, Marchant  
1057 A, Roose T (2013) High resolution synchrotron imaging of wheat root hairs growing in soil and  
1058 image based modelling of phosphate uptake. *New Phytologist* 198, 1023–1029.  
1059 doi:10.1111/nph.12294

1060 Kim, M., & Or, D. (2016). Individual-based model of microbial life on hydrated rough soil surfaces.  
1061 PLoS One, 11, e0147394. doi:10.1371/journal.pone.0147394

1062 Knutson C.E., Werth C.J., Valocchi A.J. (2005). Pore-scale simulation of biomass growth along the  
1063 transverse mixing zone of a model two-dimensional porous medium. *Water Resources Research* 41,  
1064 W07007. doi:10.1029/2004WR003459

1065 König S., Worrich A., Centler F., Wick L.Y., Miltner A., Kästner M., Thullner M., Frank K., Banitz T.  
1066 (2017). Modelling functional resilience of microbial ecosystems : Analysis of governing processes.  
1067 *Environmental Modelling & Software* 89, 31-39. doi:10.1016/j.envsoft.2016.11.025

1068 König S., Worrich A., Banitz T., Centler F., Harms H., Kästner M., Miltner A., Wick L.Y., Thullner M.,  
1069 Frank K. (2018). Spatiotemporal disturbance characteristics determine functional stability and  
1070 collapse risk of simulated microbial ecosystems. *Scientific Reports* 8, 9488. doi:10.1038/s41598-  
1071 018-27785-4

1072 König S., Köhnke M.C., Firie A-L., Banitz T., Centler F., Frank K., Thullner M. (2019). Disturbance  
1073 Size Can Be Compensated for by Spatial Fragmentation in Soil Microbial Ecosystems. *Frontiers in*  
1074 *Ecology and Evolution* 7, 290. doi:10.3389/fevo.2019.00290

1075 König S., Vogel H.J., Harms H., Worrich A. (2020). Physical, Chemical and Biological Effects on Soil  
1076 Bacterial Dynamics in Microscale Models. *Frontiers in Ecology and Evolution* 8, 53. doi:  
1077 10.3389/fevo.2020.00053

1078 Kravchenko A., Falconer R.E., Grinev D., Otten W. (2011). Fungal colonization in soils with different  
1079 management histories: modeling growth in three-dimensional pore volumes. *Ecological*  
1080 *Applications* 21, 1202-1210. doi:10.2307/23022990

1081 Kravchenko A., Guber A., Gunina A., Dippold M., Kuzyakov Y. (2020). Pore-scale view of microbial  
1082 turnover: Combining <sup>14</sup>C imaging,  $\mu$ CT and zymography after adding soluble carbon to soil pores  
1083 of specific sizes. *European Journal of Soil Science*, 1-15. doi:10.1111/ejss.13001

1084 Kravchenko, A., Otten, W., Garnier, P., Pot, V., & Baveye, P. C. (2019). Soil aggregates as  
1085 biogeochemical reactors: Not a way forward in the research on soil–atmosphere exchange of  
1086 greenhouse gases. *Global Change Biology* 25, 2205–2208. doi:10.1111/gcb.14640

1087 Laudone, G. M., Matthews, G. P., Bird, N. R. A., Whalley, W. R., Cardenas, L. M., Gregory, A. S.  
1088 (2011). A model to predict the effects of soil structure on denitrification and N<sub>2</sub>O emission. *Journal*  
1089 *of Hydrology*, 409, 283–290. doi:10.1016/j.jhydrol.2011.08.026

1090 Laudone, G. M., Matthews, G. P., Gregory, A. S., Bird, N. R. A., Whalley, W. R. (2013). A dual-porous,  
1091 inverse model of water retention to study biological and hydrological interactions in soil. *European*  
1092 *Journal of Soil Science*, 64, 345–356. doi:10.1111/ejss.12055

1093 Long T., Or D. (2005). Aquatic habitats and diffusion constraints affecting microbial coexistence in  
1094 unsaturated porous media. *Water Resources Research* 41, W08408. doi:10.1029/2004WR003796

1095 Long, T., & Or, D. (2007). Microbial growth on partially saturated rough surfaces: Simulations in  
1096 idealized roughness networks. *Water Resources Research* 43, W02409. doi:10.1029/2005WR004781

1097 Long T., Or D. (2009). Dynamics of Microbial Growth and Coexistence on Variably Saturated Rough  
1098 Surfaces. *Environmental Microbiology* 58, 262-275 doi:10.1007/s00248-009-9510-3

1099 Long W., Hilpert M. (2008). Lattice-Boltzmann modeling of contaminant degradation by chemotactic  
1100 bacteria: Exploring the formation and movement of bacterial bands. *Water Resources Research* 44,  
1101 W09415. doi:10.1029/2007WR006129

1102 Lubbers IM, Pulleman MM, van Groenigen JW (2010). Can earthworms simultaneously enhance  
1103 decomposition and stabilization of plant residue carbon? *Soil Biology and Biochemistry* 105, 12-24.  
1104 doi:10.1016/j.soilbio.2016.11.008

1105 Lugato, E., Morari, F., Nardi, S., Berti, A., Giardini, L. (2009). Relationship between aggregate pore  
1106 size distribution and organic–humic carbon in contrasting soils. *Soil & Tillage Research* 103, 153–  
1107 157. doi:10.1016/j.still.2008.10.013

1108 Masse D., Cambier C., Brauman A., Sall S., Assigbetse K., Chotte J.L. (2007). MIOR : an individual-  
1109 based model for simulating the spatial patterns of soil organic matter microbial decomposition.  
1110 *European Journal of Soil Science* 58, 1127-1135. doi:10.1111/j.1365-2389.2007.00900.x

1111 Mbé B., Monga O., Pot V., Otten W., Hecht F., Raynaud X., Nunan N., Chenu C., Baveye P.C., Garnier  
1112 P. (2021). Scenario modelling of carbon mineralization in 3D soil architecture at the microscale:  
1113 Toward an accessibility coefficient of organic matter for bacteria. *European Journal of Soil Science*.  
1114 doi:10.1111/ejss.13144

1115 Monga O., Bousso M., Garnier P., Pot V. (2008). 3D geometric structures and biological activity:  
1116 Application to microbial soil organic matter decomposition in pore space. *Ecological Modelling*  
1117 216, 291-302. doi:10.1016/j.ecolmodel.2008.04.015

1118 Monga O., Garnier P., Pot V., Coucheney E., Nunan N., Otten W., Chenu C. (2014). Simulating  
1119 microbial degradation of organic matter in a simple porous system using the 3-D diffusion-based  
1120 model MOSAIC. *Biogeosciences* 11, 2201-2209. doi:10.5194/bg-11-2201-2014

1121 Ngom N.F., Garnier P., Monga O., Peth S. (2011). Extraction of three-dimensional soil pore space from  
1122 microtomography images using a geometrical approach. *Geoderma* 163, 127–134.  
1123 doi:10.1016/j.geoderma.2011.04.013

1124 Nunan N., Schmidt H., Raynaud X. (2020). The ecology of heterogeneity: soil bacterial communities  
1125 and C dynamics. *Philosophical Transactions of the Royal Society B* 375: 20190249.  
1126 doi:10.1098/rstb.2019.0249

1127 Ortega-Ramirez P., Pot V., Laville P., Schlüter S., Hadjar D., Basile-Doelsch I., Henault C., Caurel C.,  
1128 Mazurier A., Lacoste M.; Garnier P. (2021). Role of soil microstructure on the emission of N<sub>2</sub>O in  
1129 intact small soil columns. EGU21-12438, EGU General Assembly 2021. doi:10.5194/egusphere-  
1130 egu21-12438

1131 Otten W., Gilligan C.A., Watts C.W., Dexter A.R., Hall D. (1999). Continuity of air-filled pores and  
1132 invasion thresholds for a soil-borne fungal plant pathogen, *Rhizoctonia solani*. *Soil Biology and*  
1133 *Biochemistry* 31, 1803-1810. doi:10.1016/S0038-0717(99)00099-1

1134 Otten W., Hall D., Harris K., Ritz K., Young I.M., Gilligan C.A. (2001). Soil physics, fungal  
1135 epidemiology and the spread of *Rhizoctonia solani*. *New Phytologist* 151, 459-468.  
1136 doi:10.1046/j.0028-646x.2001.00190.x

1137 Otten W., Bailey D.J., Gilligan C.A. (2004a). Empirical evidence of spatial thresholds to control  
1138 invasion of fungal parasites and saprotrophs. *New Phytologist* 163, 125-132. doi:10.1111/j.1469-  
1139 8137.2004.01086.x

1140 Otten W., Harris K., Young I.M., Ritz K., Gilligan C.A. (2004b). Preferential spread of the pathogenic  
1141 fungus *Rhizoctonia solani* through structured soil. *Soil Biology and Biogeochemistry* 36, 203-210.  
1142 doi:10.1016/j.soilbio.2003.09.006

1143 Otten W. Gilligan C.A. (2006). Soil structure and soil-borne diseases: using epidemiological concepts  
1144 to scale from fungal spread to plant epidemics. *European Journal of Soil Science* 57, 26–37.  
1145 doi:10.1111/j.1365-2389.2005.00766.x

1146 Pagel H., Kriesche B., Uksa M., Poll C., Kandeler E., Schmidt V., Streck T. (2020). Spatial Control of  
1147 Carbon Dynamics in Soil by Microbial Decomposer Communities. *Frontiers in Environmental*  
1148 *Science* 8, 2. doi: 10.3389/fenvs.2020.00002

1149 Pajor R., Falconer R., Hapca S., Otten W. (2010). Modelling and quantifying the effect of heterogeneity  
1150 in soil physical conditions on fungal growth. *Biogeosciences*, 7, 3731–3740. doi:10.5194/bg-7-  
1151 3731-2010

1152 Perez-Reche F.J., Taraskin S.N., Otten W., Viana M.P., Costa L. da F., Gilligan C.A. (2012). Prominent  
1153 effect of soil network heterogeneity on microbial invasion. *Physical Review Letters* 109, 098102.  
1154 doi:10.1103/PhysRevLett.109.098102

- 1155 Peszynska M., Trykozko A., Iltis G., Schlueter S., Wildenschild W. (2016). Biofilm growth in porous  
1156 media: Experiments, computational modeling at the porescale, and upscaling. *Advances in Water*  
1157 *Resources* 95, 288-301, doi: 10.1016/j.advwatres.2015.07.008
- 1158 Pinheiro M., Garnier P., Beguet J., Martin Laurent F., Vieublé Gonod L. (2015). The millimetre-scale  
1159 distribution of 2,4-D and its degraders drives the fate of 2,4-D at the soil core scale. *Soil Biology and*  
1160 *Biochemistry* 88, 90-100. doi:10.1016/j.advwatres.2015.07.008
- 1161 Porre RJ, van Groenigen JW, de Deyn GB, de Goede RGM, Lubbers IM (2016). Exploring the  
1162 relationship between soil mesofauna, soil structure and N<sub>2</sub>O emissions. *Soil Biology and*  
1163 *Biochemistry* 96, 55-64. doi:10.1016/j.soilbio.2016.01.018
- 1164 Portell X., Pot V., Garnier P., Otten W., Baveye P.C. (2018). Microscale Heterogeneity of the Spatial  
1165 Distribution of Organic Matter Can Promote Bacterial Biodiversity in Soils: Insights From  
1166 Computer Simulations. *Frontiers in Microbiology* 9, 1583. doi:10.3389/fmicb.2018.01583
- 1167 Pot V., Portell X., Otten W., Garnier P., Monga O., Baveye P.C. (2021). Accounting for soil architecture  
1168 and microbial dynamics in microscale models: Current practices in soil science and the path ahead.  
1169 *European Journal of Soil Science*. doi:10.1111/ejss.13142
- 1170 Quigley M.Y., Rivers M.L. and Kravchenko A.N. (2018). Patterns and Sources of Spatial  
1171 Heterogeneity in Soil Matrix From Contrasting Long Term Management Practices. *Front. Environ.*  
1172 *Sci.* 6, 28. doi: 10.3389/fenvs.2018.00028
- 1173 Rawlins, B. G., Wragg, J., Reinhard, C., Atwood, R. C., Houston, A., Lark, R. M., & Rudolph, S.  
1174 (2016). Three-dimensional soil organic matter distribution, accessibility and microbial respiration in  
1175 macroaggregates using osmium staining and synchrotron X-ray computed tomography. *The Soil* 2,  
1176 659–671. doi:10.5194/soil-2-659-2016
- 1177 Ray N., Rupp A., Prechtel A. (2017). Discrete-continuum multiscale model for transport, biomass  
1178 development and solid restructuring in porous media. *Advances in Water Resources* 107, 393-404.  
1179 doi:10.1016/j.advwatres.2017.04.001
- 1180 Resat H., Bailey V., McCue L.A., Konpka A. (2012). Modeling Microbial Dynamics in Heterogeneous  
1181 Environments : Growth on Soil Carbon Sources. *Microbial Ecology* 63, 883-897.  
1182 doi:10.1007/s00248-011-9965-x
- 1183 Rohe L., Apelt B., Vogel H-J., Well R., WU G-M., Schlüter S. (2021). Denitrification in soil as a  
1184 function of oxygen availability at the microscale. *Biogeosciences* 18, 1185–1201. doi:10.5194/bg-  
1185 18-1185-2021



1186 Rosenzweig D., Furman A., Shavit U. (2013). A Channel Network Model as a Framework for  
1187 Characterizing Variably Saturated Flow in Biofilm-Affected Soils. *Vadose Zone Journal*  
1188 doi:10.2136/vzj2012.0079

1189 Ruamps L.S., Nunan N., Chenu C. (2011). Microbial biogeography at the soil pore scale. *Soil Biology*  
1190 *and Biochemistry* 43, 280-286. doi:10.1016/j.soilbio.2010.10.010

1191 Ruiz S.A., McKay Fletcher D.M., Boghi A., Williams K.A., Duncan S.J., Scotson C.P., Petroselli C.,  
1192 Dias T.G.S., Chadwick D.R., Jones D.L., Roose T. (2020). Image-based quantification of soil  
1193 microbial dead zones induced by nitrogen fertilization. *Science of the Total Environment* 727,  
1194 138197. doi:10.1016/j.scitotenv.2020.138197

1195 Rupp A., Guhra T., Meier A., Prechtel A., Ritschel T., Ray N. and Totsche K.U. (2019). Application of  
1196 a Cellular Automaton Method to Model the Structure Formation in Soils Under Saturated  
1197 Conditions: A Mechanistic Approach. *Frontiers in Environmental Science* 7, 170. doi:  
1198 10.3389/fenvs.2019.00170

1199 Sadeghnejad S., Enzmann F., Kersten M. (2021). Digital rock physics, chemistry, and biology:  
1200 challenges and prospects of pore-scale modelling approach. *Applied Geochemistry* 131, 105028.  
1201 doi:10.1016/j.apgeochem.2021.105028

1202 Schlüter S., Eickhorst T., Mueller C.W. (2019). Correlative Imaging Reveals Holistic View of Soil  
1203 Microenvironments. *Environmental Science & Technology* 53, 829–837.  
1204 doi:10.1021/acs.est.8b05245

1205 Schimel JP (2018). Life in dry soils; Effect of drought on soil microbial communities and processes.  
1206 The Annual Review of Ecology, Evolution, and Systematics 49, 409-432. doi:10.1146/annurev-  
1207 ecolsys-110617-062614

1208 Schmidt S.I., Kreft J.H., Mackay R., Picioreanu C., Thullner M. (2018). Elucidating the impact of  
1209 micro-scale heterogeneous bacterial distribution on biodegradation. *Advances in Water Resources*  
1210 116, 67–76. doi:10.1016/j.advwatres.2018.01.013

1211 Skopp J., Jawson M.D., Doran J.W. (1990). Steady-State Aerobic Microbial Activity as a Function of  
1212 Soil Water Content. *Soil Science Society of America Journal* 54, 1619-1625.  
1213 doi:10.2136/sssaj1990.03615995005400060018x

1214 Smercina D.N., Bailey V.L., Hofmockel S. (2021). Micro on a macroscale: relating microbial-scale soil  
1215 processes to global ecosystem function. *FEMS Microbiology Ecology* 97, fiab091.  
1216 doi:10.1093/femsec/fiab091

1217 Schnepf A, Carminati A, Ahmed MA, Benard P, Bentz J, Bonkowski M, Knott M, Diehl D, Duddek P,  
1218 Kröner E, et al. (2022). Linking rhizosphere processes across scales: Opinion. *Plant and Soil*.  
1219 doi:10.1007/s11104-022-05306-7

1220 Soufan, R., Delaunay, Y., Gonod, L. V., Shor, L. M., Garnier, P., Otten, W., Baveye P.C. (2018). Pore-  
1221 scale monitoring of the effect of microarchitecture on fungal growth in a two-dimensional soil-like  
1222 micromodel. *Front. Environ. Sci.* 6:68. doi: 10.3389/fenvs.2018.00068.

1223 Stahl, P. D. & Christensen, M. (1992). In vitro interactions among members of a soil microfungus  
1224 community. *Soil Biology and Biochemistry* 24, 309–316. doi:10.1016/0038-0717(92)90190-9

1225 Šťovíček A., Kim M., Or D., Gillor O. (2017). Microbial community response to hydration-desiccation  
1226 cycles in desert soil. *Scientific Reports* 7, 45735. doi:10.1038/srep45735

1227 Strong D.T., de Wever, H., Merckx, R., Recous S. (2004). Spatial location of carbon decomposition in  
1228 the soil pore system. *European Journal of Soil Science* 55, 739–750. doi:10.1111/j.1365-  
1229 2389.2004.00639.x

1230 Tang Y., Valocchi A.J., Werth C.J., Liu H. (2013). An improved pore-scale biofilm model and  
1231 comparison with a microfluidic flow cell experiment. *Water Resources Research* 49, 8370-8382.  
1232 doi:10.1002/2013WR013843

1233 Tang, J.Y., Riley, W.J., 2013. A total quasi-steady-state formulation of substrate uptake kinetics in  
1234 complex networks and an example application to microbial litter decomposition. *Biogeosciences* 10,  
1235 8329–8351. doi:10.5194/bg-10-8329-2013

1236 Tartakovsky A.M., Scheibe T.D., Meakin P. (2009). Pore-Scale Model for Reactive Transport and  
1237 Biomass Growth. *Journal of Porous Media* 12, 417-434. doi:10.1615/JPorMedia.v12.i5.30

1238 Védère C., Vieublé-Gonod L., Pouteu V., Girardin C., Chenu C. (2020). Spatial and temporal evolution  
1239 of detritusphere hotspots at different soil moistures. *Soil Biology and Biochemistry* 150, 107975.  
1240 doi:10.1016/j.soilbio.2020.107975

1241 Vidal A., Klöffel T., Guigue J., Angst G., Steffens M., Hoeschen C., Mueller C.W. (2021). Visualizing  
1242 the transfer of organic matter from decaying plant residues to soil mineral surfaces controlled by  
1243 microorganisms. *Soil Biology and Biochemistry*, 160, 108347. doi: 10.1016/j.soilbio.2021.108347

1244 Vogel H-J., Balseiro-Romero M., Kravchenko A., Otten W., Pot V., Schlüter S., Weller U., Baveye P.C.  
1245 (2021). A holistic perspective on soil architecture is needed as a key to soil functions. *European*  
1246 *Journal of Soil Science*. doi:10.1111/ejss.13152

1247 Vogel L., Makowski D., Garnier P., Vieublé-Gonod L., Coquet Y., Raynaud X., Nunan N., Chenu C.,  
1248 Falconer R., Pot V. (2015). Modeling the effect of soil meso- and macropores topology on the  
1249 biodegradation of a soluble carbon substrate. *Advances in Water Resources* 83, 123-126.  
1250 doi:10.1016/j.advwatres.2015.05.020

1251 Vogel L.E., Pot V., Makowski D., Garnier P., Baveye P.C. (2018). To what extent do uncertainty and  
1252 sensitivity analyses help unravel the influence of microscale physical and biological drivers in soil  
1253 carbon dynamics models? *Ecological Modelling* 383, 10-22. doi:10.1016/j.ecolmodel.2018.05.007

1254 Wang B., Allison S.D (2019). Emergent properties of organic matter decomposition by soil enzymes.  
1255 *Soil Biology and Biochemistry* 136, 107522. doi:10.1016/j.soilbio.2019.107522

1256 Wang, G., & Or, D. (2010). Aqueous films limit bacterial cell motility and colony expansion on  
1257 partially saturated rough surfaces. *Environmental Microbiology*, 12, 1363–1373.  
1258 <https://doi.org/10.1111/j.1462-2920.2010.02180.x>

1259 Wang G., Or D. (2012). A Hydration-Based Biophysical Index for the Onset of Soil Microbial  
1260 Coexistence. *Scientific Reports* 2, 881. doi:10.1038/srep00881

1261 Wang G., Or D. (2013). Hydration dynamics promote bacterial coexistence on rough surfaces. *ISME*  
1262 *Journal* 7, 395-404. doi:10.1038/ismej.2012.115

1263 Wang G., Or D. (2014). Trophic interactions induce spatial self-organization of microbial consortia on  
1264 rough surfaces. *Scientific Reports* 4, 6757. doi:10.1038/srep06757

1265 Wieder W.R., Allison S.D., Davidson E.A., Georgiou K., Hararuk O., He Y., Hopkins F., Luo Y., Smith  
1266 M.J., Sulman B., Todd-Brown K., Wang Y-P., Xia J., Xu X. (2015). Explicitly representing soil  
1267 microbial processes in Earth system models. *Global Biogeochemical Cycles* 29, 1782-1800.  
1268 doi:10.1002/2015GB005188.

1269 Yan Z., Liu C., Todd-Brown K.E., Liu Y., Bond-Lamberty B., Bailey V.L. (2016). Pore-scale  
1270 investigation on the response of heterotrophic respiration to moisture conditions in heterogeneous  
1271 soils. *Biogeochemistry* 131, 121-134. doi:10.1007/s10533-016-0270-0

1272 Yan Z., Wang T., Wang L., Yang X., Smith P., Hilpert M., Li S., Shang J., Bailey V., Liu C. (2018).  
1273 Microscale water distribution and its effects on organic carbon decomposition in unsaturated soils.  
1274 *Science of the Total Environment* 644, 1036-1043. doi:10.1016/j.scitotenv.2018.06.365

1275 Zech S., Ritschel T., Ray N., Totsche K.U., Prechtel A. (2022). How water connectivity and substrate  
1276 supply shape the turnover of organic matter – Insights from simulations at the scale of  
1277 microaggregates. *Geoderma* 405, 115394. doi:10.1016/j.geoderma.2021.115394

# Understanding the joint impacts of soil architecture and microbial dynamics on soil functions: insights derived from microscale models

Pot, Valérie

2022-06-23

Attribution-NonCommercial 4.0 International

---

Pot V, Portell X, Otten W, et al., (2022) Understanding the joint impacts of soil architecture and microbial dynamics on soil functions: insights derived from microscale models. *European Journal of Soil Science*, Volume 73, Issue 3, May-June 2022, Article number e13256

<https://doi.org/10.1111/ejss.13256>

*Downloaded from CERES Research Repository, Cranfield University*